

Primordial Magnetic Field Effects on the CMB and Large Scale Structure

Dai G. Yamazaki^{1,*}, Kiyotomo Ichiki², Toshitaka Kajino^{3,4}, and Grant J. Mathews⁵

¹*Institute of Astronomy and Astrophysics, Academia Sinica,*

7F of Condensed Matter Sciences and Physics Department Building,

National Taiwan University.No.1, Roosevelt Rd, Sec. 4 Taipei 10617, Taiwan, R.O.C

²*Department of Physics and Astrophysics, Nagoya University, Nagoya 464-8602, Japan*

³*National Astronomical Observatory of Japan, Mitaka, Tokyo 181-8588, Japan*

⁴*Department of Astronomy, Graduate School of Science,*

The University of Tokyo, Hongo 7-3-1, Bunkyo-ku, Tokyo 113-0033, Japan and

⁵*Center for Astrophysics, Department of Physics,*

University of Notre Dame, Notre Dame, IN 46556, U.S.A.

(Dated: December 3, 2010)

Magnetic fields are everywhere in nature and they play an important role in every astronomical environment which involves the formation of plasma and currents. It is natural therefore to suppose that magnetic fields could be present in the turbulent high temperature environment of the big bang. Such a primordial magnetic field (PMF) would be expected to manifest itself in the cosmic microwave background (CMB) temperature and polarization anisotropies, and also in the formation of large-scale structure. In this review we summarize the theoretical framework which we have developed to calculate the PMF power spectrum to high precision. Using this formulation, we summarize calculations of the effects of a PMF which take accurate quantitative account of the time evolution of the cut off scale. We review the constructed numerical program, which is without approximation, and an improvement over the approach used in a number of previous works for studying the effect of the PMF on the cosmological perturbations. We demonstrate how the PMF is an important cosmological physical process on small scales. We also summarize the current constraints on the PMF amplitude B_λ and the power spectral index n_B which have been deduced from the available CMB observational data by using our computational framework.

INTRODUCTION

Many astrophysical and cosmological phenomena in the universe are affected by magnetic fields over a broad range of scales. Indeed, magnetic fields with a strength of $B \sim 1.0 \mu G$ have been detected [1–3] even on scales as large as that of galactic clusters. Such magnetic fields are frozen-in to the ionized baryons. The magnetic energy density scales as $B^2 \propto a^{-4}$ while the baryon density scale as $\rho \propto a^{-3}$. Hence, we can relate the field strength to the cosmic density $B^3 \propto \rho^2$. Considering that clusters of galaxies observed today would have isotropically-collapsed relative to the background density, a cluster magnetic field of $B \sim 1.0 \mu G$ would correspond to a primordial magnetic field (PMF) of order $\sim 1.0 nG$ at the epoch of photon last scattering, $z \sim 1100$.

The origin of such a cosmological primordial magnetic field has been an area of active research by many authors. One expects that such a field would have a random distribution of orientations and field strength. If the PMF has a nearly scale invariant spectrum, an origin from vector potentials generated during the inflation epoch is one of the best candidates [4–6]. Cosmological phase transitions could also produce a PMF with a bluer spectrum [7–10]. Several authors have also discussed magnetic field generation on smaller scales during or after the epoch of photon last scattering ($z \lesssim 1100$) [11–13]. Since each model for the generation of the PMF involves different length scales, the spectral index of the PMF power spectrum, n_B correlates with the generation models. Therefore, constraining n_B can lead to constraints on models for the generation of the PMF.

A primordial magnetic field (PMF) affects electrons and protons through the Lorentz force. Subsequently, ionized baryons affect photons through Thomson scattering. In this way the PMF affects photons indirectly in the early universe. A number of studies in the literature [14–40] have analyzed effects of a fiducial PMF of order $\sim 1 nG$ on the matter power spectrum as well as the temperature fluctuations and polarization anisotropies of the cosmic microwave background (CMB). Many others have been, also been attempting to constrain the strength of the PMF by various means, e.g. the non-gaussianity of the temperature fluctuations of CMB[41–43], Faraday rotation effects[44–47], CMB anomalies[36, 48, 49], and effects on large scale structure (LSS) [50, 51]. These studies have indicated that the PMF effects are mainly manifest on the smallest scales in the linear regime, i.e. before the formation of nonlinear structure. This is of interest because, there are possible discrepancies between observation and theory in the linear regime on small angular scales which could be attributable to a PMF. However, to accurately estimate the influence of not only a PMF but also non-linear effects, it is crucial to have the proper tools to constrain the PMF from cosmological observations. The purpose of this review is to summarize the development of such tools.

We have developed methods [25–29, 32] to analyze the effects of a PMF on the matter and CMB power spectra. The parameters characterizing the PMF have then been constrained from a fit [38] to the observational data. By simultaneously fitting the matter and CMB contributions, we have shown that a more comprehensive and accurate model for the PMF effects in cosmology can be obtained. This allows for improved constraints on the parameters characterizing the PMF.

In section II of this review we will introduce the basic cosmological physics of the PMF and in sections III and IV we will discuss its effects on the matter power spectrum and CMB. In section V we will discuss the results of a search for constraints on parameters of the PMF from observations of the matter power spectra and CMB. In section IV we will also explore the possibilities for new physics to be obtained from a better understanding of the PMF, e.g. contributions of the PMF to the gravitational wave mode (BB-mode).

THE MODEL

In this section we review how to model the effects of a PMF on the cosmic fluid. We assume a flat Friedmann-Robertson-Walker (FRW) background cosmology for the linear perturbations and adopt a conformal synchronous gauge as in Ref. [25]. Hence, the line element is given [25] by

$$ds^2 = a^2(\tau)[-d\tau^2 + (\delta_{ij} + h_{ij})dx^i dx^j], \quad (1)$$

where the x^i are spatial coordinates, $a(\tau)$ is the scale factor, h_{ij} is the metric perturbation around the background spacetime, and τ is the conformal time defined by:

$$\tau \equiv \int_0^t \frac{dt'}{a(t')}. \quad (2)$$

Here and in the following we use natural units $c = \hbar = 1$ except where otherwise noted.

Primordial Magnetic Field

In order to solve the perturbed Einstein Equations it is first necessary to specify the energy momentum tensor for the magnetic field. We can adopt a prior upper limit on the PMF amplitude of order $\simeq 1.0 - 10$ nG based upon observations of magnetic fields on the scale of galactic clusters as described below. Fortunately, for a PMF of order $1.0 - 10$ nG at the surface of photon last scattering, the total energy density in the PMF is smaller than the energy density in the temperature fluctuations of the CMB. Therefore, we can treat the energy density of the PMF as a first order perturbation and assume a stiff source for the time evolution. By a stiff source we mean that all back reactions from the fluid onto the magnetic field can be discarded because these are second order perturbations. In this case, we can also assume that the conductivity of the primordial plasma is very large and that the electric field is negligible, i.e. $E \sim 0$. This "frozen-in" condition is a very good and useful approximation [15].

On the largest scales the time evolution of the PMF can be decoupled from its spatial dependence, i.e., $\mathbf{B}(\tau, \mathbf{x}) = \mathbf{B}_0(\mathbf{x})/a^2$. This leads to the following simplified electromagnetic energy-momentum tensor,

$$T^{00}_{[\text{EM}]}(\mathbf{x}, \tau) = \frac{B(\mathbf{x})^2}{8\pi a^6} , \quad (3)$$

$$T^{i0}_{[\text{EM}]}(\mathbf{x}, \tau) = T^{0k}_{[\text{EM}]}(\mathbf{x}, \tau) = 0 , \quad (4)$$

$$-T^{ik}_{[\text{EM}]}(\mathbf{x}, \tau) = \sigma_B^{ik} = \frac{1}{8\pi a^6} \{2B^i(\mathbf{x})B^k(\mathbf{x}) - \delta^{ik}B(\mathbf{x})^2\} . \quad (5)$$

When dealing with cosmological fluctuations, it is convenient to work in k -space and denote all quantities by their Fourier transform convention $F(\mathbf{k}) = \int d^3x \exp(i\mathbf{k} \cdot \mathbf{x})F(\mathbf{x})$, where k is a wave number. Just as for the CMB temperature fluctuations, a PMF that is statistically homogeneous, isotropic and random, the fluctuation power spectrum can be parameterized as a power-law $P(k) \propto k^{n_B}$ [15, 24] where n_B is the spectral index.

The electromagnetic stress-energy tensor in k space is given by [25],

$$T_j^i(\mathbf{k})_{[\text{EM}]} = \frac{1}{4\pi a^4} \int \frac{d^3k'}{(2\pi)^3} \left\{ \frac{1}{2} \delta_j^i B^l(\mathbf{k}') B_l(\mathbf{k} - \mathbf{k}') - B^i(\mathbf{k}') B_j(\mathbf{k} - \mathbf{k}') \right\} . \quad (6)$$

When comparing with observations, one desires a statistical measure of the fluctuations on various scales. For this, it is best to work with a two-point correlation function for the PMF which then be defined [15] by

$$\langle B^i(\mathbf{k}) B^{j*}(\mathbf{k}') \rangle = \frac{(2\pi)^{n_B+8}}{2k_\lambda^{n_B+3}} \frac{B_\lambda^2}{\Gamma\left(\frac{n_B+3}{2}\right)} k^{n_B} P^{ij}(k) \delta(\mathbf{k} - \mathbf{k}') , \quad k < k_C , \quad (7)$$

where $B_\lambda = |\mathbf{B}_\lambda|$ is the strength of the comoving mean magnetic field derived by smoothing over a Gaussian sphere of comoving radius λ and $k_\lambda = 2\pi/\lambda$ (with $\lambda = 1$ Mpc here). The tensor $P^{ij}(k)$ is defined by $P^{ij}(k) = \delta^{ij} - k^i k^j / k^2$. The damping scale from radiative viscosity provides a natural cutoff wave number k_C in the PMF magnetic power spectrum. It is defined in Refs.[52–54].

We have evolved the PMF source power spectrum using the numerical methods described in Refs. [25, 29]. Using this method, we have quantitatively evaluated the time evolution of the cut off scale, and hence, more reliably calculated the effects of a PMF.

Cosmological fluids, curvature fluctuations, and the PMF

Cosmological perturbations can be either of a scalar form (fluctuations in energy density), vector form (momentum fluctuations), or tensor form (T^{ij} fluctuations). Considering the scalar mode first, the ionized baryons (electrons and protons) in the early universe are influenced by PMF Lorentz forces. Before the epoch of photon last scattering ($z > 1100$), the photons are immersed in a fluid of ionized baryons along with the PMF and are indirectly affected by the PMF through Thomson scattering. At the same time, the matter and radiation respond to the background curvature fluctuations η . We have found that it is very important to carefully account for the dependence of the curvature fluctuations on the conformal time τ up to at least second order, $\mathcal{O}(\tau^2)$. This is because there is a cancellation between contributions from the primordial magnetic field and primordial radiation at first order. Fortunately, higher than first order $\mathcal{O}(\tau)$ terms of $\eta(\tau)$ can be included by considering the matter contributions to the scale factor a [55, 56],

$$a \simeq \sqrt{\frac{8\pi G \rho_{R0}}{3}} \tau + \frac{8\pi G \rho_{M0}}{12} \tau^2 = \alpha\tau + \beta\tau^2 \quad (8)$$

where, ρ_{R0} and ρ_{M0} are total energy densities in radiation and matter, respectively. A model without this matter contributions may give some values which are mathematically close to the correct answer for a limited range of time and length scales. However, such models are not physically correct. In fact, by neglecting this coupling, the curvature perturbation η of the scalar mode of our previous numerical estimation [29] was too small to stabilize the numerical calculation for large scales and early times. This problem is illustrated in Figure 1 which shows a comparison (for $B_\lambda = 1.0$ nG and $n_B = -2.9$) of the CMB temperature fluctuations in the scalar mode with and without a consideration of the matter contributions to the scale factor. Since the previous curvature perturbation η was too small and there was an instability in the numerical calculations for large scales and early times, the CMB temperature fluctuations for lower ℓ rise higher without the matter contributions to a than a calculation with matter contributions. In order to solve this problem, we have adopted the model of Ref. [56] for estimating the effects of the PMF on fluctuations of the scalar mode in the early universe. We have also utilized adiabatic initial conditions for the matter contributions as in Ref. [56]. This leads to stable numerical calculations of the curvature perturbations of the scalar mode for all length scales and times. This is an improvement over previous numerical estimates for which the scalar curvature perturbations were too small to be stabilized in the numerical calculations for large scales and early times. Thus, our current method allows one to obtain consistent results for all scales and times of interest.

Correlations between the PMF and the Primary Density Field

Many authors have studied models for the origin of the PMF. However, there is little consensus yet as to the true origin of the PMF. Because of this, we cannot be certain of how the PMF correlates with fluctuations of the primordial density field. Nevertheless, one can define a parameter "s" to denote how much the power spectrum of the PMF correlates with fluctuations of the primordial density field [25, 28].

In the linear regime, the power spectra of density fluctuations in the baryons ($P_b(k)$) and cold dark matter ($P_{\text{CDM}}(k)$) in the presence of a PMF are as follows,

$$P_b(k) = \left\langle \delta_{[\text{b:FL}]}(k) \delta_{[\text{b:FL}]}^*(k) \right\rangle + \left\langle \delta_{[\text{b:PMF}]}(k) \delta_{[\text{b:PMF}]}^*(k) \right\rangle + 2 \left\langle \delta_{[\text{b:FL}]}(k) \delta_{[\text{b:PMF}]}^*(k) \right\rangle, \quad (9)$$

$$P_{\text{CDM}}(k) = \left\langle \delta_{[\text{CDM:FL}]}(k) \delta_{[\text{CDM:FL}]}^*(k) \right\rangle + \left\langle \delta_{[\text{CDM:PMF}]}(k) \delta_{[\text{CDM:PMF}]}^*(k) \right\rangle + 2 \left\langle \delta_{[\text{CDM:FL}]}(k) \delta_{[\text{CDM:PMF}]}^*(k) \right\rangle, \quad (10)$$

where the brackets denote the various two-point correlation functions as defined above, and δ_α and $\alpha \in ([\text{b:FL}], [\text{CDM:FL}])$ designate the baryon and CDM density fluctuations without the PMF, respectively. While, δ_β and $\beta \in ([\text{b:PMF}], [\text{CDM:PMF}])$ denote the baryon and CDM density fluctuations with the PMF included (without the primary fluctuations). In this power spectrum we normalize the cross correlation terms with the parameter s,

$$\left\langle \delta_{[\text{b:FL}]}(k) \delta_{[\text{b:PMF}]}^*(k) \right\rangle \equiv s \sqrt{\left\langle \delta_{[\text{b:FL}]}(k) \delta_{[\text{b:FL}]}^*(k) \right\rangle \left\langle \delta_{[\text{b:PMF}]}(k) \delta_{[\text{b:PMF}]}^*(k) \right\rangle}, \quad (11)$$

$$\left\langle \delta_{[\text{CDM:FL}]}(k) \delta_{[\text{CDM:PMF}]}^*(k) \right\rangle \equiv s \sqrt{\left\langle \delta_{[\text{CDM:FL}]}(k) \delta_{[\text{CDM:FL}]}^*(k) \right\rangle \left\langle \delta_{[\text{CDM:PMF}]}(k) \delta_{[\text{CDM:PMF}]}^*(k) \right\rangle}. \quad (12)$$

When $0 < s \leq 1$, $s = 0$, or $-1 \leq s < 0$ in eqs.(11) and (12), one has positive, vanishing, or negative correlations, respectively.

Next, the Boltzmann equation can be utilized to find the equations of for the baryons as the follows,

$$\dot{v}_b = -\frac{\dot{a}}{a} v_b + c_s^2 k^2 \delta_b + \frac{4\bar{\rho}_\gamma}{3\bar{\rho}_b} a n_e \sigma_T (v_\gamma - v_b) + k^2 \frac{\rho_{\gamma 0}}{a \rho_{b0}} \frac{\Pi_{[\text{EM:S}]}(\mathbf{k})}{4\pi \rho_{\gamma 0}}, \quad (13)$$

where v_b and v_γ are the baryon and photon velocity perturbations, δ_b and δ_γ are the baryon and photon density perturbations, c_s is the sound speed, n_e is the free electron density, σ_T is the Thomson scattering cross section, ρ_{b0} and $\rho_{\gamma 0}$ are baryon and photon densities, and $\Pi_{[\text{EM:S}]}(\mathbf{k})$ is the square root of the power spectrum function for the Lorentz force (given in [25]).

The Lorenz force term in Eq.(13) can be divided into two terms, the magnetic pressure and the tension. By comparing those terms, one can decide which of them is dominant in the Lorenz force. There is, however, no

information as to whether the magnetic pressure or the tension is dominant, and whether the direction of the forces from them are the same or different. Nevertheless, such information should be taken into account when it can be determined from a model. To see how these pieces arise, we summarize the derivation of the scalar Lorentz force term as given in Ref. [25]. Analogous derivations of the vector and tensor two-point correlation functions can be found in Ref. [29]. One can first rewrite the two-point correlation function for the scalar part of the electromagnetic energy tensor in k space as,

$$\begin{aligned} \langle T_{[\text{EM:S}]}(\mathbf{k}) T_{[\text{EM:S}]}^*(\mathbf{k}') \rangle &= \hat{k}_i \hat{k}^j \hat{k}_l \hat{k}^m \langle T_j^i([\text{EM}](\mathbf{k})) T_m^{*l}([\text{EM}](\mathbf{k}') \rangle \\ &= (2\pi)^3 |\Pi_{[\text{EM:S}]}(\mathbf{k})|^2 \delta(\mathbf{k} - \mathbf{k}') \quad , \end{aligned} \quad (14)$$

where $\Pi_{[\text{EM:S}]}(\mathbf{k})$ is the power spectrum of the Lorenz force that we wish to analyze.

One can next decompose the electromagnetic stress-energy tensor in k space into two parts as follows,

$$T_j^i(\mathbf{k})_{[\text{EM}]} = T_j^i(\mathbf{k})_{[\text{EM:1}]} - T_j^i(\mathbf{k})_{[\text{EM:2}]} \quad (15)$$

$$T_j^i(\mathbf{k})_{[\text{EM:1}]} = \frac{1}{4\pi a^4} \int \frac{d^3 k'}{(2\pi)^3} \frac{1}{2} \delta_j^i B^l(\mathbf{k}') B_l(\mathbf{k} - \mathbf{k}') \quad (16)$$

$$T_j^i(\mathbf{k})_{[\text{EM:2}]} = \frac{1}{4\pi a^4} \int \frac{d^3 k'}{(2\pi)^3} B^i(\mathbf{k}') B_j(\mathbf{k} - \mathbf{k}') \quad (17)$$

Correspondingly, one can define [25] $T_{[\text{EM:S1}]} = \hat{k}_i \hat{k}^j T_j^i([\text{EM:1}]$ and $T_{[\text{EM:S2}]} = \hat{k}_i \hat{k}^j T_j^i([\text{EM:2}]$. Using Eq.(15 - 17), one can finally rewrite the two point correlation function for the scalar part of the Lorenz force as,

$$\begin{aligned} \langle T(\mathbf{k})_{[\text{EM:S}]} T^*(\mathbf{k}')_{[\text{EM:S}]} \rangle &= \langle (T(\mathbf{k})_{[\text{EM:S1}]} - T(\mathbf{k})_{[\text{EM:S2}]}) (T^*(\mathbf{k}')_{[\text{EM:S1}]} - T^*(\mathbf{k}')_{[\text{EM:S2}]}) \rangle \\ &= \langle T(\mathbf{k})_{[\text{EM:S1}]} T^*(\mathbf{k}')_{[\text{EM:S1}]} \rangle - \langle T(\mathbf{k})_{[\text{EM:S1}]} T^*(\mathbf{k}')_{[\text{EM:S2}]} \rangle \\ &\quad - \langle T(\mathbf{k})_{[\text{EM:S2}]} T^*(\mathbf{k}')_{[\text{EM:S1}]} \rangle + \langle T(\mathbf{k})_{[\text{EM:S2}]} T^*(\mathbf{k}')_{[\text{EM:S2}]} \rangle. \end{aligned} \quad (18)$$

The first term on the R.H.S. can be identified as the magnetic pressure while the fourth term is the magnetic tension. The second and third terms are the cross correlation. A key part of the analysis of the effects of the PMF on the cosmic fluid is to understand the relative roles of these terms.

Fig. 2 shows the ratio of the magnetic pressure to the tension as in the Lorentz force term [25] as a function of the spectral index n_B . The pressure dominates when $n_B < -1.5$, while the tension is slightly larger when $n_B > -1.5$.

The sign of the cross correlation terms depends upon the relative signs of the pressure and tension. In order to determine the relative signs of these two terms, however, one must specify a model for the generation of the PMF. There is as of yet no consensus model. Therefore, we decompose the factors into various possible combinations, i.e.

$$s = s_{[\text{LF}]} \times s_{[\text{DF}]}, \quad (19)$$

where

$$s_{[\text{LF}]} = \begin{cases} -1, & n < -1.5 \quad (\text{I}), \\ -1, & n > -1.5 \quad (\text{II}), \\ 1, & n > -1.5 \quad (\text{III}), \end{cases} \quad (20)$$

and

$$\begin{aligned} 0 &< s_{[\text{DF}]} \leq 1 \quad (\text{i}), \\ s_{[\text{DF}]} &= 0 \quad (\text{ii}), \\ -1 &\leq s_{[\text{DF}]} < 0 \quad (\text{iii}). \end{aligned}$$

In the different regimes, $s_{[\text{LF}]}$ represents either: (I) the pressure dominated case; (II) the tension dominated case, where the magnetic field pressure and tension forces act in the same direction; or (III) the tension dominated case, where the magnetic field pressure and tension forces act in the opposite direction. On the other hand, $s_{[\text{DF}]}$ represents either: (i) a positive correlation between the matter and PMF distributions; (ii) no correlation; or (iii) a negative correlation. Thus, if $s < 0$, the matter and PMF distributions could be correlated positively ($s_{[\text{DF}]} > 0$) and the PMF pressure dominates in the Lorentz term (for $n < -1.5$). Another possibility is that the matter and PMF distributions negatively correlate ($s_{[\text{DF}]} < 0$) and the PMF tension dominates in the Lorentz term (for $n > -1.5$) and the tension acts on the density field in the same direction as the magnetic field pressure. Yet another possibility is that the PMF tension dominates in the Lorentz term ($n > -1.5$), but the tension acts on the density field in the opposite direction

from the pressure force. In these cases the PMF effects act like a gas pressure to oppose the gravitational collapse and therefore causes the density perturbations to more slowly evolve.

On the other hand, if $s > 0$, the matter and PMF distributions could positively correlate ($s_{[\text{DF}]} > 0$) and the PMF tension dominates in the Lorentz term ($n > -1.5$) while the tension acts on the density field in the opposite direction from the pressure force. Alternatively, the matter and PMF distributions could negatively correlate ($s_{[\text{DF}]} < 0$) and the PMF pressure dominates in the Lorentz term ($n < -1.5$). In these cases the Lorentz force from the PMF accelerates the gravitational collapse. After decoupling, δ does not oscillate and the perturbation evolution is straightforward for all of the above cases.

EFFECTS OF A PMF ON THE MATTER POWER SPECTRUM

In this section we review the effects of the PMF on fluctuations in the matter density on cosmological scales (see [25] for details).

Effects of a PMF on the Matter Density Field

Figure 3 shows that the density fluctuations of matter are more strongly affected by a PMF for wavenumbers $k/h > 0.1 \text{ Mpc}^{-1}$ [25]. This is because the energy density of the PMF, E_B , only depends upon the scale factor as a^{-4} like the photons, and unlike the photons, the magnetic field fluctuations can survive on scales below the photon diffusion length, i.e. below the Silk damping scale. Since the CDM and baryons interact with each other through gravity, the Lorentz force from the PMF can also indirectly affect the cold dark matter (CDM). This effect on the CDM is much smaller than that on the baryons before the epoch of photon last scattering because the density of baryons oscillates with that of photons and their gravitational effect on the CDM is very small. After the epoch of photon last scattering, the time evolution of the CDM density starts to be influenced by the baryon density through gravitational interaction [57]. Therefore, the Lorentz force effect of the PMF on the CDM increases with time.

The strength of this effect is dependent upon the ratio of the baryon density to the CDM density, Ω_b/Ω_c . The density fluctuations of the baryons are directly generated by the PMF, while the density fluctuations of the CDM are indirectly generated from the gravitational interaction with the baryons. Therefore, the density fluctuations of the CDM only grow due to gravitational instability, and their growth rate is nearly the same as the density fluctuations of the primordial CDM. On the other hand, the evolution of the baryon density fluctuations is not dominated by the gravitational potential until the gravity becomes comparable to the Lorentz force, i.e. $4\pi G\rho\delta \sim k^2 \frac{\Pi_{[\text{EM:S}]}(\mathbf{k}, \tau)}{4\pi\rho_b}$, where $\Pi_{[\text{EM:S}]}(\mathbf{k}, \tau)$ is the Lorentz force power spectrum [25]. This is because the baryons density fluctuations are generated by the PMF directly. As mentioned above, the effect of a PMF on the baryon density fluctuations is largest on the smallest scales (larger k values). Hence, the density fluctuations for baryons in the presence of a PMF increase with the wavenumber k [25].

Matter Power Spectra with a PMF

It should be noted that the effect of a PMF on the matter power spectrum, $P(k)$ is different from effect of a PMF on the matter density fluctuations δ . The fluctuations of total density δ can become smaller or larger depending upon whether the dominant effect is from the pressure or the tension of the PMF. On the other hand, the effects of a PMF upon the matter power spectrum are dependent on how well the spectrum of the PMF correlates with the primary density fluctuations.

Figure 3 illustrates the degeneracy between the PMF-matter-density correlation factor $s_{[\text{DF}]}$ and the PMF spectral index n_B . This figure shows that a change of spectral index from $n_B = -2.0$ to -1.0 can be offset by including a negative correlation. The correlation factor $s_{[\text{DF}]}$, however, depends upon the origin of the PMF. We will discuss the below the resolution of this degeneracy problem, along with the relation between the correlation factor $s_{[\text{DF}]}$ and the origin of the PMF.

Negative correlation of the density perturbations

In the case of a negative correlation between the PMF and the matter density fluctuations, the pressure of the PMF accelerates the evolution of the fluctuations in the matter density, while the tension of the PMF delays them. Thus, for $n < -1.5$, for which the pressure of the PMF dominates, the PMF accelerates the evolution of the matter density fluctuations. On the other hand, for $n > -1.5$, for which the tension dominates, the PMF delays the evolution. If we assume that the PMF would have been produced in low density regions, such negative correlations might be allowed. This situation, however, is difficult to realize for a causally produced PMF, because it seems natural that more amplitude for the PMF would be generated in regions with higher matter density and therefore higher currents.

No correlation

The PMF and the matter density fluctuations are uncorrelated when $s_{\text{[DF]}} = 0$. The PMF then increases the matter power spectrum independently of whether the pressure or tension dominate the PMF. If density fluctuations generate the PMF as in Ref. [13], peaks in the amplitude of the PMF should lie at peaks in the pressure gradient of the cosmological fluids. In this case, the PMF is produced along the border between high and low density regions, i.e., $\delta \sim 0$. Eventually, such a PMF has no (or very weak) statistical correlation with fluctuations in the matter density.

Positive correlation

In the case of a positive correlation between the PMF and fluctuations in the matter density, the evolution of the matter density fluctuations is accelerated by the tension of the PMF. Therefore, the matter evolution is delayed by the pressure of the PMF. Thus, for $n < -1.5$, for which the pressure of the PMF dominates, the evolution of the matter density fluctuations is delayed by the PMF. On the other hand, for $n > -1.5$, a PMF accelerates the evolution. If we assume that the PMF would have been produced in higher density regions, such positive correlations might be allowed.

EFFECTS OF A PMF ON THE CMB

In this section, we review effects of a PMF on the temperature fluctuations and polarization anisotropies of the CMB (see [29, 38] for details). Regarding the CMB polarization, the reader should be aware that in cosmology the intensity of polarized radiation is expressed in terms of two scalar fields E and B that are independent of how the coordinate system is oriented. E and B are the curl-free and curl-like components of the linear polarization field. Based upon these there are three types of fluctuations: scalar, vector and tensor. There are then four observables: the temperature, E -mode, B -mode, and the temperature cross polarization power spectra. From these, one can generate three power spectra TT, EE, and BB, where T is the total intensity and also three cross-spectra TE, TB, and EB. However, the only nonzero spectra are TT, EE, BB, and TE due to parity considerations.

Figures 4 - 6 show that the usual (TT mode) CMB power spectra for large multipoles ℓ (small angular scale) are influenced most strongly by the PMF. The first reason for this is that the energy density of the PMF scales with the cosmic expansion as a^{-4} just like the photons, Unlike photons, however, the magnetic fields are not much affected by photon diffusion. As a result, the temperature fluctuations and polarization anisotropies of the CMB continue to be affected by a PMF even for angular scales smaller than the Silk damping scale. Another reason is that a dominant contribution to the CMB on smaller angular scales comes from the vector mode of the PMF. This is because, after horizon crossing, the scalar mode cannot evolve due to the acoustic oscillations. That is, the photons fall in and out of gravitational potentials but cannot grow. On the other hand, the vector mode of the PMF fluctuations can continue growing once inside the horizon. For higher ℓ , the vector mode also dominates the CMB polarization from the PMF, and the tensor mode from the PMF diminishes [cf. figures 4 - 6][17, 29, 38, 58]. The gravitational waves generated by the PMF can be negligibly small after horizon crossing. This is because this homogeneous solution starts to oscillate inside the horizon and decay rapidly [59–62]. Consequently, the anisotropy spectrum is affected by gravity waves only on scales larger than the horizon at the epoch of photon last scattering.

Panel (b) on figure 4 and figure 6 show that the BB mode from the PMF can dominate for $B_\lambda \gtrsim 2.0$ nG for multipoles with $\ell \gtrsim 200$. On these angular scales there is also the BB mode which is converted from the EE power spectrum by gravitational lensing [62]. Therefore, there is a degeneracy between the PMF and gravitational lensing

on small angular scales. However, since the spectrum from the effects of the gravitational lensing signal have been independently determined, this power can be subtracted directly. We have shown [29, 38] that the effects of a PMF on the temperature fluctuations of the CMB are stronger with correlations than without, as is also the case for the matter power spectrum with a PMF. This is illustrated in Figure 5.

There is also a degeneracy between the Sunyaev-Zel'dovich effect and the PMF. Nevertheless, the effects of a PMF on the CMB are independent of frequency because the PMF influences the primary CMB as a background. Eventually, by using observations at different frequencies, it should be possible to distinguish the effects of a PMF from foreground effects which depend upon frequency.

CONSTRAINTS ON THE PMF

In this section, we review constraints on the parameters of the PMF from cosmological observations. First, we show that a strong constraint on the PMF amplitude and spectral index can be derived from the prior observed constraints on the σ_8 parameter. This fiducial quantity represents the root-mean-square of the matter density fluctuation in a comoving sphere of radius $8h^{-1}$ Mpc and as such is a measure of the growth of large scale structure. It is given by a weighted integral over the matter power spectrum [63]. Second, we note that the parameters of the PMF can be strongly constrained by using the observational data on the CMB with the previous priors used in the analysis of Refs. [64–66] without a PMF. In the last subsection, we will discuss the possible origins of a PMF based upon the deduced constraints on the parameters characterizing the PMF.

Prior on the PMF Parameters from σ_8

Because of the degeneracy of affects on the observed CMB power spectrum from various parameters, it has become standard in the field of CMB physics to fit the CMB parameters by a Bayesian method that makes optimum use of the variety of independently determined constraints on cosmological parameters. For this purpose the Monte-Carlo Markov Chain (MCMC)[67] analysis has become the method of choice to find the multidimensional surface of maximum likelihood among the many parameters. In this context we note that the PMF amplitude B_λ and power law index n_B have a strong degeneracy. Therefore, one must identify a strong prior constraint to effectively decouple these two parameters of the PMF. In this quest we are aided by observed constraints on the σ_8 parameter for which a value of $0.7 < \sigma_8 < 0.9$ has been deduced from diverse observational data on linear cosmological scales[68–71]. Using this range as a prior in the Monte-Carlo Markov Chain (MCMC)[67] analysis, constraints on the parameters of the PMF can be obtained by a fit to the observed power spectra of the CMB. For some of the cosmological parameters, Ω_b , Ω_{CDM} , n_S , and A_S affect σ_8 , we also have to consider the possible degeneracy between these cosmological parameters and the PMF parameters. Fortunately, however, recent observations of the CMB have constrained such cosmological parameters on larger scales ($\ell < 1000$) [64–66]. As mentioned above, the PMF mainly affects the CMB anisotropies on smaller scales ($\ell > 1000$)[25, 26, 29]. Therefore, only a small degeneracy between the PMF parameters and the other cosmological parameters is expected, so that fixing the other cosmological parameters at the WMAP best fit values is justified.

Figure 7 and the panels in Figure 8 show the optimum PMF parameters n_B and B_λ for various constant values of σ_8 as labeled. Since the PMF power spectrum depends upon k^{2n_B+3} [29], for $n_B < -1.5$, the PMF effects on the density fluctuations for smaller scales decrease with lower values for n_B . Therefore since σ_8 depends upon the amplitude of the matter power spectrum for smaller scale, when the spectral index is near $n_B = -3.0$, the matter power spectrum in the presence of a PMF is smaller for smaller scales. Thus, larger amplitudes of B_λ are allowed. For $n_B > -1.5$, however, the energy density power spectrum of the PMF is proportional to the cut-off scale $k_C^{2n_B+3}$ [29]. k_C is also, proportional to $B_\lambda^{-1/(n_B+5)}$ [29, 52–54]. Substituting these relations into Eqs.(15)-(17) in Ref. [29], we easily obtain the following relation between the PMF power spectrum and the magnetic field strength, $P(k)_{\text{PMF}} \propto B_\lambda^{[14/(n_B+5)]}$. Considering $B_\lambda \ll 1\text{G}$, the matter power spectrum with the PMF for $n_B > -1.5$ becomes larger for larger n_B . Therefore larger amplitudes of B_λ are not allowed for larger n_B .

Since the effects of a PMF for negative and positive correlations change at $n_B = -1.5$ (see Section), we divide the discussion below of each correlation into two parts based upon whether the spectral index is greater or less than $n_B = -1.5$.

No Correlation

As mentioned above in Sub-Section., in the case of no correlation between the PMF and the density fluctuations from primary perturbations, the effect of a PMF is to increase the matter power spectrum independently of whether the pressure or tension dominates the PMF. As noted above, from recent constraints on the σ_8 parameter from cosmological observations of LSS we can exclude PMF parameters which imply $\sigma_8 > 1$.

Hence, we can exclude a PMF with field strength $B_\lambda \gtrsim 1$ nG if $n_B > -0.9$ (Fig. 7). We can also exclude a PMF with amplitude $B_\lambda \gtrsim 0.1$ nG if $n_B > 0.2$. If we assume that the origin of the observed magnetic field in the clusters of galaxies is the PMF, we can limit the PMF amplitude to $B_\lambda \gtrsim 1$ nG. In this case, we can exclude a PMF spectral index in the range $n_B > -0.9$.

Negative Correlation

As noted above in subsection , in the case of a negative correlation, the tension of the PMF delays the evolution of the matter density fluctuations, while the pressure tends to accelerate them. Furthermore, the pressure of the PMF dominates for $n_B < -1.5$, while the tension of the PMF dominates for $n_B > -1.5$. Therefore, for $n < -1.5$ the matter density fluctuations are accelerated by the PMF, while, for $n > -1.5$, this evolution is delayed by the PMF. This behavior can be traced to the third terms in both Eqs.(11) and (12). Using the allowed range of PMF parameters as mentioned above, we can exclude the range of PMF amplitude to $B_\lambda \gtrsim 1$ nG if $n_B > -0.81$, and the range of PMF amplitudes to $B_\lambda \gtrsim 0.1$ nG if $n_B > 0.26$ (panels (a-1) and (a-2) in Figure 8). However, as mentioned above, it is difficult to model the production of a PMF in matter fields of low energy density in order to realize such negative correlations.

Positive Correlation

As noted above in Sub-Section., in the case of a negative correlation, the pressure of the PMF delays the evolution of the matter density fluctuations while the tension accelerates them. Considering the same conditions as in the previous section.V A 1, the PMF decreases the fluctuations of matter density for $n_B < -1.5$. On the other hand, for $n_B > -1.5$, it increases the fluctuations. In this case, we can exclude the range of PMF amplitudes with $B_\lambda \gtrsim 1$ nG if $n_B > -0.94$, and the range of PMF amplitudes with $B_\lambda \gtrsim 0.1$ nG for $n_B > 0.13$ (panels (b-1) and (b-2) in Figure 8).

Constraint on the PMF from the CMB

In this section, we summarize the current constraints on parameters of the PMF from fits to the CMB and LSS observational data. We consider a flat ($k = 0$) Λ CDM universe characterized by 8 parameters, i.e. $\{\Omega_b h^2, \Omega_c h^2, \tau_C, n_s, \log(10^{10} A_s), A_t/A_s, |B_\lambda|, n_B\}$, where $\Omega_b h^2$ and $\Omega_c h^2$ are the baryon and CDM densities in units of the critical density, h denotes the Hubble parameter in units of $100 \text{ km s}^{-1} \text{ Mpc}^{-1}$, τ_C is the optical depth for Compton scattering, n_s is the spectral index of the primordial scalar fluctuations, A_s is the scalar amplitude of the primordial scalar fluctuations and A_t is the scalar amplitude of the primordial tensor fluctuations. We define the tensor index for the primordial tensor fluctuations as $n_t = -(A_s/A_t)/8$. For all cosmological parameters we use the same prior constraints as those adopted in the WMAP analysis [72]. As noted in the previous section, the case of no correlation is more realistic than the case of negative or positive correlations. Therefore, we focus here on the constraints of the parameters characterizing the PMF in the case of no correlation.

Using the MCMC algorithm and available cosmological observations, we have constrained the standard cosmological parameters and the PMF parameters listed in Table.1. We note, however, that the MCMC algorithm tends to sparsely sample near a boundary, and hence find low probability there. This is why it appears that n_B is constrained even in the limit that $B_\lambda \rightarrow 0$. Of course, for $B_\lambda = 0$ there is no constraint on the spectral index at all. This shortcoming, however, does not negate the fact that there is a genuine minimum in the goodness of fit for a finite magnetic field and spectral index. In the optimum fit with the inclusion of parameters of the PMF, the minimum total χ^2 changes from 2803.4 to 2800.2 corresponding to a change in the χ^2 per degree of freedom from 1.033 to 1.031. Therefore, a finite PMF slightly improves the goodness of fit even after taking into account the new degrees of freedom. The existence of a PMF, however, is still only of marginal significance.

Figures 9 and 10 show the 68% and 95% C.L. probability contours in the planes of various cosmological parameters versus the amplitude $|B_\lambda|$, or power law index n_B , along with the probability distributions. Figure 10 and the bottom panels in Fig. 9 show the probability distributions for $|B_\lambda|$ and n_B . Of particular note for this review is the presence of maxima in the likelihood functions for $|B_\lambda| = 0.85 \pm 1.25$ nG and $n_B = -2.37^{+0.88}_{-0.73}$. Although these values are consistent with zero magnetic field, and thus only imply upper limits, they suggest the possibility that with forthcoming data (particularly for large CMB multipoles) a finite magnetic field may soon be detectable.

These figures exhibit no degeneracy between the PMF parameters and the standard cosmological parameters. Table 1 confirms that the standard cosmological parameters are not significantly different from those deduced directly from the WMAP 5yr data analysis without a PMF. The reason for this is simple. The standard cosmological parameters are mainly constrained by the observed CMB power spectrum for low multipoles $\ell < 1000$ (up to the 2nd acoustic peak). On the other hand, the PMF dominates for $\ell > 1000$. Hence, the PMF effect on the power spectrum is nearly independent of the standard cosmological parameters.

The tensor to scalar ratio A_t/A_s deduced in our analysis is smaller than the upper limit $A_t/A_s < 0.43$ (95% CL) deduced from the WMAP 5yr data analysis without a PMF. The reason for this is that we define A_t as the tensor amplitude of the primary CMB spectrum (without a PMF). This tensor term only arises from the primordial gravitational-wave background produced during inflation. We combine the tensor amplitude from the PMF and A_t when we compare our tensor amplitude with the result deduced by others. The value of A_t by itself is comparable to the tensor contribution from the PMF. The value of A_t/A_s from the WMAP 5yr data is less than 0.43 (95% CL). Hence, our result is consistent with the previous constraints when the additional PMF contribution is included.

The degeneracy of the PMF parameters [26] is broken by the different effects of the PMF on both the matter power spectrum and the CMB power spectrum. The vector mode can dominate for higher ℓ in the CMB temperature anisotropies [29], while the matter power spectrum becomes sensitive [25] to the power law spectral index n_B when a PMF is present. Additionally, the CMB fluctuations from the PMF are smaller than the primary CMB fluctuations for the scalar and tensor modes on large angular scales [30, 31]. Therefore, the tensor to scalar ratio is not affected by the PMF.

Figure 11 shows our deduced probability distributions and the 1σ and 2σ (68% and 95% C.L.) probability contours for the resultant cosmological parameters, σ_8 , H_0 , z_{reion} , and Age. Here, $H_0 = 100h$ km s $^{-1}$ Mpc $^{-1}$ is the Hubble parameter, z_{reion} is the red shift at which re-ionization occurs, and Age is the presently observed age of the universe in Gyr. It is important to keep in mind that these parameters are not input parameters, but are output results. The sum of the results on Figures 9 - 11 provides marginal evidence that both upper and lower limits to the parameters of the PMF can be deduced.

Table 1 summarizes the upper limits to the PMF parameters with input and output cosmological parameters, σ_8 , H_0 , z_{reion} , and Age. In particular we find that $|B_\lambda| < \mathbf{2.10}$ (68%CL) nG and $< \mathbf{2.98}$ (95%CL) nG and $n_B < \mathbf{-1.19}$ (68%CL) and $< \mathbf{-0.25}$ (95%CL) at a present scale of 1 Mpc. Although previous work [25, 26, 29, 32] could obtain a less stringent upper limit to $|B_\lambda|$ they could not constrain n_B at all. Moreover, our deduced probability distributions suggests that a finite PMF provides the best fit.

On angular scales smaller than that probed by the CMB the observed number density of galaxies is a better measure of the power spectrum. Therefore, since the PMF mainly influences the small angular scales, using the combined LSS observational data (2dFDR[68]), and the CMB (WMAP 5yr[73], ACBAR[74], CBI[75], Boomerang[76]) we can constrain the PMF better than in previous works which relied on the CMB data only. In particular, an upper limit on n_B can be constrained for the first time while the lower limit to n_B is approaching the 1σ confidence level.

The right-bottom panel of Figure 9 shows that the maximum likelihood is for a spectral index of $n_B = -2.4^{+0.9}_{-0.7}$. It is important [26, 77] to constrain n_B as this parameter provides insight into models for the formation of the PMF. If the PMF were formed during inflation one would expect a scale-invariant value of $n_B = -3$. The value deduced in Figures 8-11 and Table 1, are thus consistent with an inflation generated PMF at the 1σ confidence level.

Next we discuss other generation models for the PMF during various phase transitions [7–10] from the gravity waves produced along with the PMF. The formation of light elements during big-bang nucleosynthesis (BBN) depends upon a balance between the nuclear reaction rates and the expansion rate of the universe. Since gravity waves contribute to the total energy density they affect the expansion rate. Hence, they are constrained by a comparison between the BBN predictions and the observed light element abundances [26, 77]. There are also other theoretical constraints on the origin of the PMF. For example, in Ref. [78] it was noted that a non-scale-invariant spectrum of the PMF is difficult to generate or survive if it is formed via a causal mechanism during later phase transitions. Indeed, as pointed out in Ref. [77, 78] the spectral index of a magnetic field generated during any period of standard Friedmann expansion (i.e. any time except inflation) is constrained to be a positive even integer larger than two: $n_B = 2, 4, 6, \dots$. This constraint, which applies for example to a PMF generated at a phase transition, or by second order MHD processes and so on, comes simply from the fact that the magnetic field generation is a causal process (i.e. the universe has a

<i>Cosmological Parameters</i>		
Parameter	mean	best fit
$\Omega_b h^2$	0.02320 ± 0.00059	0.02295
$\Omega_c h^2$	0.1094 ± 0.0046	0.1093
τ_C	0.087 ± 0.017	0.082
n_s	0.977 ± 0.016	0.970
$\ln(10^{10} A_s)$	3.07 ± 0.036	3.06
A_t/A_s	$< 0.170(68\%CL), < 0.271(95\%CL)$	0.0088
$ B_\lambda (\text{nG})$	$< \mathbf{2.10}(68\%CL), < \mathbf{2.98}(95\%CL)$	0.85
n_B	$< \mathbf{-1.19}(68\%CL), < \mathbf{-0.25}(95\%CL)$	-2.37
σ_8	$0.812^{+0.028}_{-0.033}$	0.794
H_0	73.3 ± 2.2	72.8
z_{reion}	10.9 ± 1.4	10.5
Age(Gyr)	13.57 ± 0.12	13.62

TABLE I. PMF parameters and Λ CDM model parameters and 68% confidence intervals (A_t/A_s is a 95% CL) from a fit to the WMAP[73] + ACBAR[74] + CBI[75] + Boomerang[76] + 2dFDR[68] data.

finite horizon at the magnetic field generation time). Based upon this, the fact our results favor a negative spectral index near -3, indicate that an inflation mechanism [4–6] may be the most likely origin for the PMF.

A PMF affects not only the temperature fluctuations, but also the polarization of the CMB. Although we fit all available polarization data, it turns out that the TT and BB modes (where T is the temperature fluctuation and B is the curl-like component of polarization) are the most important. Figures 12 and 13 show a comparison of the computed best-fit total power spectrum with the observed CMB spectrum. Plots show various spectra for the TT and BB modes. We plot the best fit and allowed regions both including the SZ effect (scattering from re-ionized electrons) at the K(22.8GHz) band (upper curves) and without the SZ effect (lower curves) in Figure 11. Including the SZ effect only slightly diminishes the best fit magnitude of the PMF. Although the CBI point falls about 1σ above the best fit, the χ^2 is dominated by the better ACBAR08 data and this point does not significantly affect the deduced PMF parameters.

DISCUSSION

Effects of a PMF on the early universe have been studied by a number of researchers including ourselves. A summary of some of the relevant topics and their implications for different PMF field strengths is given in Table 2. For example, in the first row, if a PMF originated during a post inflation epoch, its strength is probably $|B_\lambda| \ll 1nG$, while if it was generated during inflation its field strength at the surface of last photon scattering was likely $|B_\lambda| \sim 1nG$. Furthermore the BB mode of the CMB from the tensor component is strongly affected by the gravitational wave background. Therefore, the BB mode also shows characteristics of the gravitational wave background from the PMF and an inflation origin. If the PMF has a field strength order of $1 nG$, then from figure 5 and 6, we expect that the gravity wave background (without the PMF) dominates the BB mode for smaller $\ell < 200$, while, the PMF dominates this mode for $\ell > 200$. Hence, if the gravity wave background without the PMF is generated by inflation, the origin of the gravity wave background on large scales will be inflation, while the background for smaller scales is from the PMF.

Based upon the current status of the field, we can summarize the following: 1) A PMF mainly affects the CMB temperature fluctuations and polarization anisotropies for small angular scales; 2) Fits to observations of the CMB polarization anisotropies for small angular scales are generally better when effects of the PMF are included; and 3) A PMF can either increase or decrease the matter density fluctuations on scales less than that of galaxy clusters.

Comparison with other determinations

As noted above, in our previous numerical estimate [29], the curvature perturbations of the scalar mode were too small to stabilize the numerical calculations for large scales and early times. This is caused by an unwanted cancellation between contributions from the primordial magnetic field and the primordial radiation fields which seemed to imply excess power for the lowest multipoles of the CMB. In order to solve this problem, we have adopted the numerical approach and initial conditions for the matter contributions from Ref. [79]. This formulation has been developed

independently and gives consistent results for large scales and early times. We have now confirmed that our results are consistent not only with results of Ref. [79], but also those of other groups which employ semi-numerical methods [e.g. Ref. [30]].

Influence of the PMF on Large Scale Structure

In Ref. [38] we deduced the effects of a PMF on the matter energy density fields by considering a stochastic PMF that depends upon scale. We then quantitatively discussed the effect of a PMF on the seeds of LSS in the early universe. We have also considered more general effects of the PMF than those considered in previous work. For example, we included not only the magnetic field tension but also the increases in pressure and energy density perturbations from the field. Furthermore, by considering the correlation between the PMF and the matter density fluctuations, and utilizing mathematically exact stochastic PMF power spectrum sets, we have obtained reasonable and accurate models for the evolution of baryons, CDM, and photons, and therefore, the large scale structure. We have shown [38] that the PMF can play a very different role on the evolution of density perturbations depending upon how the PMF and matter fluctuations are correlated. We have also considered the fact that after decoupling, the CDM is influenced indirectly by the PMF through gravitational interaction.

We reported in Ref. [29] that a PMF on small angular scales ($\lambda \approx 1\text{Mpc}$) and a field strength of $B_\lambda \sim 1\text{ nG}$ [15, 17, 18, 26, 27, 80] provides a new interpretation for the excess of CMB anisotropies for high multipoles. We showed that if a PMF with such strength was present, it is very likely that it has affected the formation of large scale structure. In Ref. [81] it was suggested that in order to avoid false coupling between the baryons and the CDM on small scales, one should use independent transfer functions for the baryons and CDM. A PMF would be another source of this difference in the transfer function for baryons and the CDM. Since the density perturbations in the early universe have evolved to the present LSS, the evolution of the LSS with a PMF becomes different from that without a PMF. We have shown that the baryon and CDM energy density perturbations evolve very differently in the presence of a PMF; and with the PMF taken into consideration, the evolution of large scale structure becomes more complicated.

Future Observations

Magnetic fields affect the generation and evolution of a wide variety of cosmological and stellar objects in the universe, e.g. galaxy clusters, galaxies, primordial stars, etc., (cf. Table 2). Therefore, it is important to constrain the parameters characterizing the PMF in order to study their effects on physical processes in the universe. In this regard, forthcoming missions, e.g. QUIET, PolarBear, and Planck are expected to provide much more precise data on the CMB temperature and polarization anisotropies. At the same time data on the formation of large scale structure will continue to be measured more precisely both by future space-based observations and from continuing ground-based observations such as the SDSS and 2dF projects.

As summarized in this review, at the present time, we now understand the main effects of a PMF on both the CMB and the matter power spectrum. The important task remaining in the future will be to apply our new and correct numerical methods for calculating all PMF fluctuations of the scalar, vector and tensor modes in the TT and BB power spectra (see figures 11, 12 and 13) to fit the new observations as they emerge. Only through a critical

Topics	$ B_\lambda \ll 1nG$	$ B_\lambda \sim 1nG$
the origin of PMF	post-inflation	Inflation
the gravitational wave background	Inflation	Large scale $F_{\text{inflation}}$ Small scale F_{PMF}
the formation of LSS	necessity of some generation model for the magnetic field or vorticity	necessity for proper initial conditions considering the magnetic field and vorticity
the magnetic field in clusters of galaxies	necessity of some global magnetic field generation mode + amplification model	PMF origin
the re-ionization and the first objects	—	Formation of the first stars and the re-ionization are stimulated by a PMF.

TABLE II. Effects of the PMF on each physical processes

comparison with such future data can we hope to ultimately clarify the magnitude and origin of the PMF in the early universe.

Although, some degeneracy between the standard cosmological and PMF parameters is expected in the present data, we believe that by simultaneously investigating both the CMB anisotropies and matter power spectra one can resolve these degeneracies. The ultimate establishment of the existence and properties of a PMF will permit a better understanding of its generation and evolution and also provide new insight into the formation of LSS as well as a possible new probe of the physics of the early universe.

This work has been supported in part by Grants-in-Aid for Scientific Research (20105004, 20244035, 21740177, 20169444) of the Ministry of Education, Culture, Sports, Science and Technology of Japan. This work is also supported by the JSPS Core-to-Core Program, International Research Network for Exotic Femto Systems (EFES). Work at UND supported in part by the US Department of Energy under research grant DE-FG02-95-ER40934.

Initial conditions

In this Appendix, we introduce the initial conditions of compensated magnetic modes with massless neutrinos in the synchronous gauge which were derived by Ref.[56]. Subscripts in this appendix indicate the standard cosmological species: γ : photon, ν : massless neutrino, b: baryon, and CDM: cold dark matter. We define the density closure parameters as the ratios of density parameter as $\Omega_x = \rho_x/\rho_{\text{cr}}$, where ρ_{cr} is the critical density of the universe and the subscript x denotes the various species listed above. We also define ratios of $R_\gamma = \Omega_\gamma/\Omega_{\text{r}}$, $R_\nu = \Omega_\nu/\Omega_{\text{r}}$, and $R_{\text{b}} = \Omega_{\text{b}}/\Omega_{\text{m}}$, where $\Omega_{\text{r}} = \Omega_\gamma + \Omega_\nu$ and $\Omega_{\text{m}} = \Omega_{\text{CDM}} + \Omega_{\text{b}}$.

scalar mode

Potential

$$h = -3R_\gamma \frac{\beta}{\alpha} \tau + \frac{9}{2} R_\gamma \frac{\beta^2}{\alpha^2} \tau^2 + \mathcal{O}(\tau^3) \quad (21)$$

Curvature potential

$$\eta = \frac{1}{2} R_\gamma \frac{\beta}{\alpha} \tau + \left[\frac{R_\nu R_\gamma}{6(4R_\nu + 15)} k^2 - \frac{3}{4} R_\gamma \frac{\beta^2}{\alpha^2} \right] \tau^2 + \mathcal{O}(\tau^3) \quad (22)$$

Density perturbations

$$\delta_{\text{CDM}}^{(\text{S})} = -\frac{3}{4} R_\gamma + \frac{3}{2} R_\gamma \frac{\beta}{\alpha} \tau - \frac{9}{4} R_\gamma \frac{\beta^2}{\alpha^2} \tau^2 + \mathcal{O}(\tau^3) \quad (23)$$

$$\delta_\gamma^{(\text{S})} = -R_\gamma + 2R_\gamma \frac{\beta}{\alpha} \tau - \left(\frac{R_\nu}{6} k^3 + 3R_\gamma \frac{\beta^2}{\alpha^2} \right) \tau^2 + \mathcal{O}(\tau^3) \quad (24)$$

$$\delta_\nu^{(\text{S})} = -R_\gamma + 2R_\gamma \frac{\beta}{\alpha} \tau + \left(\frac{R_\nu}{6} k^3 - 3R_\gamma \frac{\beta^2}{\alpha^2} \right) \tau^2 + \mathcal{O}(\tau^3) \quad (25)$$

$$\delta_{\text{b}}^{(\text{S})} = \frac{3}{4} \delta_\gamma^{(\text{S})} \quad (26)$$

Velocity perturbations

$$v_\gamma^{(\text{S})} = \frac{1}{4} R_\nu k \tau + \frac{1}{4} (1 - 2R_\nu - 3R_{\text{b}} R_\nu + R_\nu^2) \frac{\beta}{\alpha} k \tau^2 + \mathcal{O}(\tau^3) \quad (27)$$

$$v_\nu^{(\text{S})} = \frac{1}{4} R_\gamma k \tau + \frac{1}{4} R_\gamma \frac{\beta}{\alpha} k \tau^2 + \mathcal{O}(\tau^3) \quad (28)$$

$$v_{\text{b}}^{(\text{S})} = v_\gamma^{(\text{S})} \quad (29)$$

Anisotropic stress

$$\Pi_\nu^{(\text{S})} = -\frac{3R_\gamma}{4R_\nu + 15} k^2 \tau^2 + \mathcal{O}(\tau^3) \quad (30)$$

Boltzmann hierarchy of neutrinos

$$F_{\nu 3}^{(\text{S})} = -\frac{R_\gamma}{4R_\nu + 15} k^3 \tau^3 + \mathcal{O}(\tau^4) \quad (31)$$

vector mode

Vector potential

$$\sigma^{(V)} = \frac{15R_\gamma}{56R_\nu + 210}k\tau - \frac{225R_\gamma}{7(8R_\nu^2 + 90R_\nu + 225)}\frac{\beta}{\alpha}k\tau^2 + \mathcal{O}(\tau^3) \quad (32)$$

Velocity perturbations

$$v_\gamma^{(V)} = -\frac{1}{8}k\tau + \frac{3R_b}{8R_\gamma}\frac{\beta}{\alpha}k\tau^2 + \mathcal{O}(\tau^3) \quad (33)$$

$$v_\nu^{(V)} = -\frac{R_\gamma}{8R_\nu}k\tau + \mathcal{O}(\tau^3) \quad (34)$$

$$v_b^{(V)} = v_\gamma^{(V)} \quad (35)$$

Anisotropicstress

$$\Pi_\nu^{(V)} = -\frac{R_\gamma}{R_\nu} + \frac{45R_\gamma}{56R_\nu^2 + 210R_\nu}k^2\tau^2 + \mathcal{O}(\tau^3) \quad (36)$$

Boltzmann hierarchy of neutrinos

$$F_{\nu 3}^{(V)} = -\sqrt{\frac{2}{3}}\frac{R_\gamma}{R_\nu}k\tau + \mathcal{O}(\tau^3) \quad (37)$$

tensor mode

tensor potential

$$\mathcal{H}^{(T)} = \frac{5R_\gamma}{28(4R_\nu + 15)}k^2\tau^2 + \mathcal{O}(\tau^3) \quad (38)$$

Anisotropicstress

$$\Pi_\nu^{(T)} = -\frac{R_\gamma}{R_\nu} + \frac{15R_\gamma}{56R_\nu^2 + 210R_\nu}k^2\tau^2 + \mathcal{O}(\tau^3) \quad (39)$$

Boltzmann hierarchy of neutrinos

$$F_{\nu 3}^{(T)} = -\frac{\sqrt{5}}{2}\frac{R_\gamma}{R_\nu}k\tau + \mathcal{O}(\tau^3) \quad (40)$$

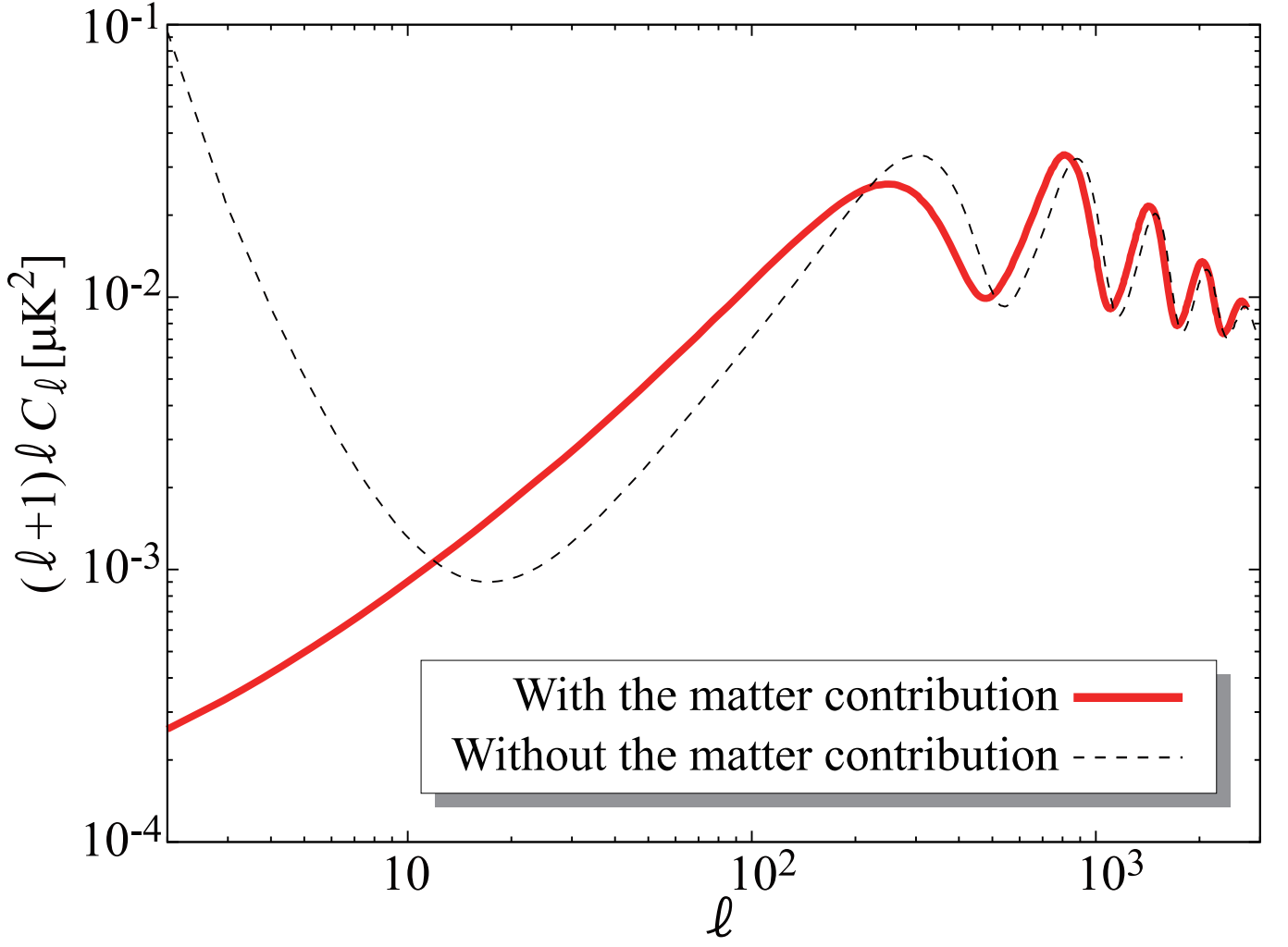


FIG. 1. Comparison of CMB temperature fluctuations from the scalar mode with (red thick curve) and without (thin dashed curve) terms of $\mathcal{O}(\tau^2)$ from the matter contributions to the scale factor. For this plot we have set $B_\lambda = 1.0$ nG and $n_B = -2.9$.

* yamazaki@asiaa.sinica.edu.tw

- [1] A. M. Wolfe, K. M. Lanzetta, and A. L. Oren, *ApJ*. **388**, 17 (1992).
- [2] T. E. Clarke, P. P. Kronberg, and H. Boehringer, *Astrophys. J.* **547**, L111 (2001).
- [3] Y. Xu, P. P. Kronberg, S. Habib, and Q. W. Dufton, *Astrophys. J.* **637**, 19 (2006).
- [4] M. S. Turner and L. M. Widrow, *Phys. Rev. D* **37**, 2743 (1988).
- [5] B. Ratra, *Astrophys. J.* **391**, L1 (1992).
- [6] K. Bamba and J. Yokoyama, *Phys. Rev. D* **70**, 083508 (2004).
- [7] T. Vachaspati, *Phys. Lett. B* **265**, 258 (1991).
- [8] T. W. B. Kibble and A. Vilenkin, *Phys. Rev. D* **52**, 679 (1995).
- [9] J. Ahonen and K. Enqvist, *Phys. Rev. D* **57**, 664 (1998).
- [10] M. Joyce and M. E. Shaposhnikov, *Phys. Rev. Lett.* **79**, 1193 (1997).
- [11] K. Takahashi, K. Ichiki, H. Ohno, and H. Hanayama, *Phys. Rev. Lett.* **95**, 121301 (2005).
- [12] H. Hanayama et al., *Astrophys. J.* **633**, 941 (2005).
- [13] K. Ichiki, K. Takahashi, H. Ohno, H. Hanayama, and N. Sugiyama, *Science* **311**, 827 (2006).
- [14] K. Subramanian and J. D. Barrow, *Phys. Rev. Lett.* **81**, 3575 (1998).
- [15] A. Mack, T. Kahniashvili, and A. Kosowsky, *Phys. Rev. D* **65**, 123004 (2002).
- [16] K. Subramanian and J. D. Barrow, *Mon. Not. Roy. Astron. Soc.* **335**, L57 (2002).
- [17] A. Lewis, *Phys. Rev. D* **70**, 043011 (2004).
- [18] D. G. Yamazaki, K. Ichiki, and T. Kajino, *Astrophys. J.* **625**, L1 (2005).

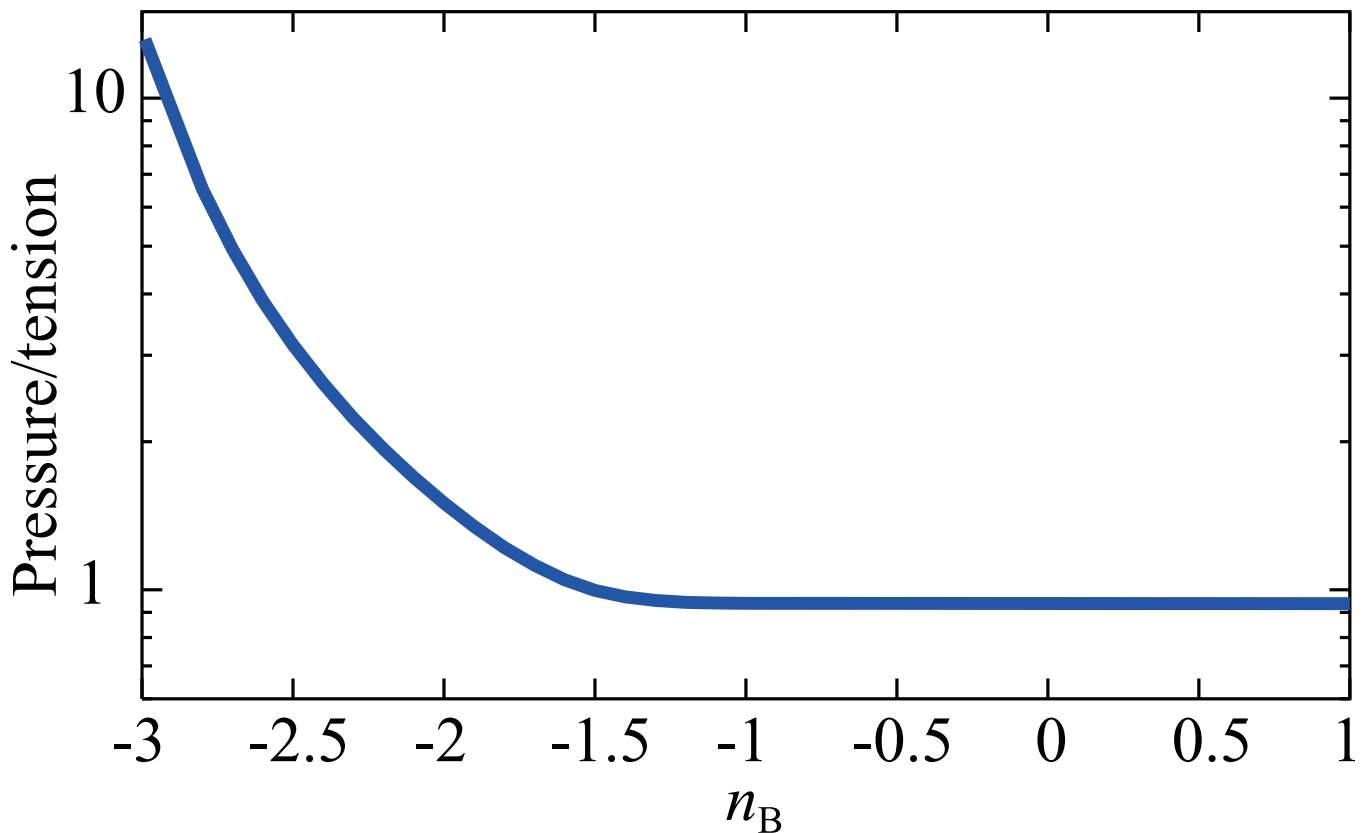


FIG. 2. Ratio of stochastic PMF pressure and tension sources. For illustration the cut off scale k_C was fixed to $k_c = 10 \text{ Mpc}^{-1}$. The pressure dominates for $n_B < -1.5$, and the magnetic tension dominates for $n_B > -1.5$.

- [19] T. Kahniashvili and B. Ratra, Phys. Rev. **D 71**, 103006 (2005).
- [20] A. Challinor, Lect. Notes Phys. **653**, 71 (2004).
- [21] A. D. Dolgov (2005), astro-ph/0503447.
- [22] R. Gopal and S. K. Sethi, Phys. Rev. **D 72**, 103003 (2005).
- [23] D. G. Yamazaki, K. Ichiki, and T. Kajino, Nuclear Physics A **758**, 791 (2005).
- [24] T. Kahniashvili and B. Ratra, Phys. Rev. **D75**, 023002 (2007).
- [25] D. G. Yamazaki, K. Ichiki, K. I. Umezu, and H. Hanayama, Phys. Rev. **D 74**, 123518 (2006).
- [26] D. G. Yamazaki, K. Ichiki, T. Kajino, and G. J. Mathews, Astrophys. J. **646**, 719 (2006).
- [27] D. G. Yamazaki, K. Ichiki, T. Kajino, and G. J. Mathews, PoS(NIC-IX). p. 194 (2006).
- [28] M. Giovannini, Phys. Rev. **D 74**, 063002 (2006).
- [29] D. G. Yamazaki, K. Ichiki, T. Kajino, and G. J. Mathews, Phys. Rev. **D 77**, 043005 (2008).
- [30] D. Paoletti, F. Finelli, and F. Paci, Mon. Not. Roy. Astron. Soc. **396**, 523 (2009).
- [31] F. Finelli, F. Paci, and D. Paoletti, Phys. Rev. **D78**, 023510 (2008), 0803.1246.
- [32] D. G. Yamazaki, K. Ichiki, T. Kajino, and G. J. Mathews, Phys. Rev. **D 78**, 123001 (2008).
- [33] D. G. Yamazaki, K. Ichiki, T. Kajino, and G. J. Mathews, PoS(NIC-X). p. 239 (2008).
- [34] S. K. Sethi, B. B. Nath, and K. Subramanian, Mon. Not. Roy. Astron. Soc. **387**, 1589 (2008).
- [35] K. Kojima, K. Ichiki, D. G. Yamazaki, T. Kajino, and G. J. Mathews, Phys. Rev. **D78**, 045010 (2008).
- [36] T. Kahniashvili, G. Lavrelashvili, and B. Ratra, Phys. Rev. **D78**, 063012 (2008).
- [37] M. Giovannini and K. E. Kunze, Phys. Rev. **D78**, 023010 (2008), 0804.3380.
- [38] D. G. Yamazaki, K. Ichiki, T. Kajino, and G. J. Mathews, Phys. Rev. **D 81**, 023008 (2010).
- [39] D. G. Yamazaki, K. Ichiki, T. Kajino, and G. J. Mathews, Phys. Rev. **D 81**, 103519 (2010).
- [40] D. G. Yamazaki, K. Ichiki, T. Kajino, and G. J. Mathews, AIP Conference Proceedings **1269**, 57 (2010).
- [41] I. Brown and R. Crittenden, Phys. Rev. **D 72**, 063002 (2005).
- [42] T. R. Seshadri and K. Subramanian, Phys. Rev. Lett. **103**, 081303 (2009).
- [43] C. Caprini, F. Finelli, D. Paoletti, and A. Riotto, JCAP **0906**, 021 (2009).
- [44] A. Kosowsky and A. Loeb, Astrophys. J. **469**, 1 (1996).
- [45] T. Kolatt, Astrophys. J. **495**, 564 (1998).
- [46] A. Kosowsky, T. Kahniashvili, G. Lavrelashvili, and B. Ratra, Phys. Rev. **D 71**, 043006 (2005).
- [47] L. Campanelli, A. D. Dolgov, M. Giannotti, and F. L. Villante, Astrophys. J. **616**, 1 (2004).

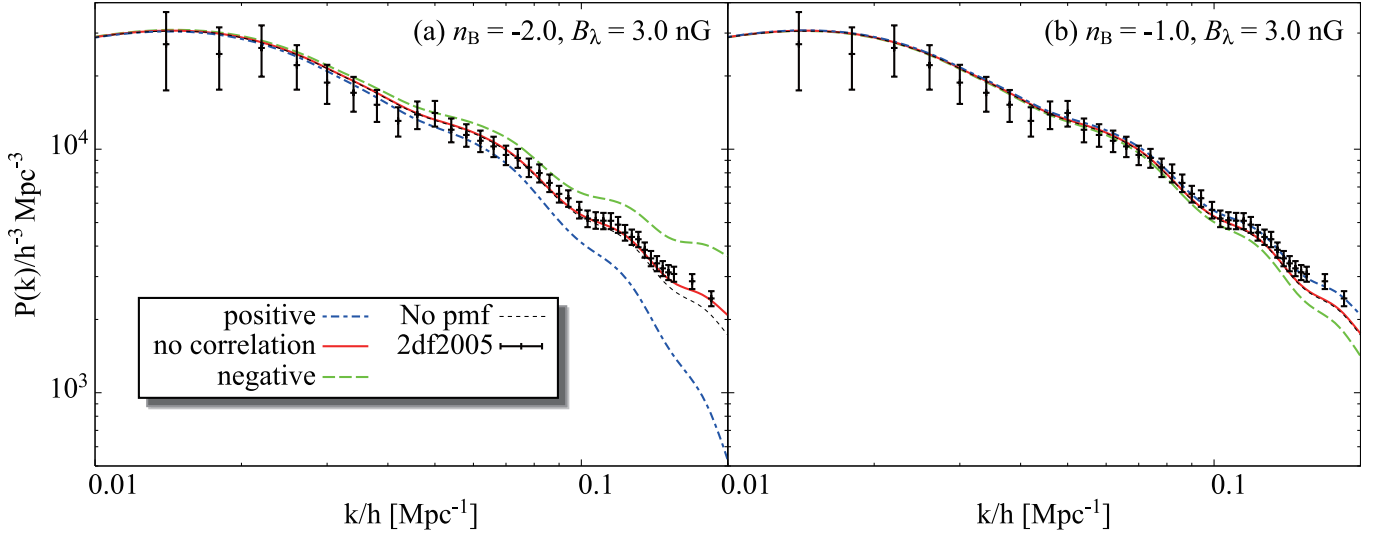


FIG. 3. Effects on the matter power spectra of the PMF. The left and right panels are for $n_B = -2.0$ and -1.0 . The green-dashed, red-bold, and blue-dotted-dashed curves are the case of negative ($s_{[\text{DF}]} = -1$), no ($s_{[\text{DF}]} = 0$) and positive ($s_{[\text{DF}]} = 1$) correlations between the matter and PMF, respectively. A Black-dotted curve is the matter power spectrum without a PMF and the dots with error bars show the 2df results[68]

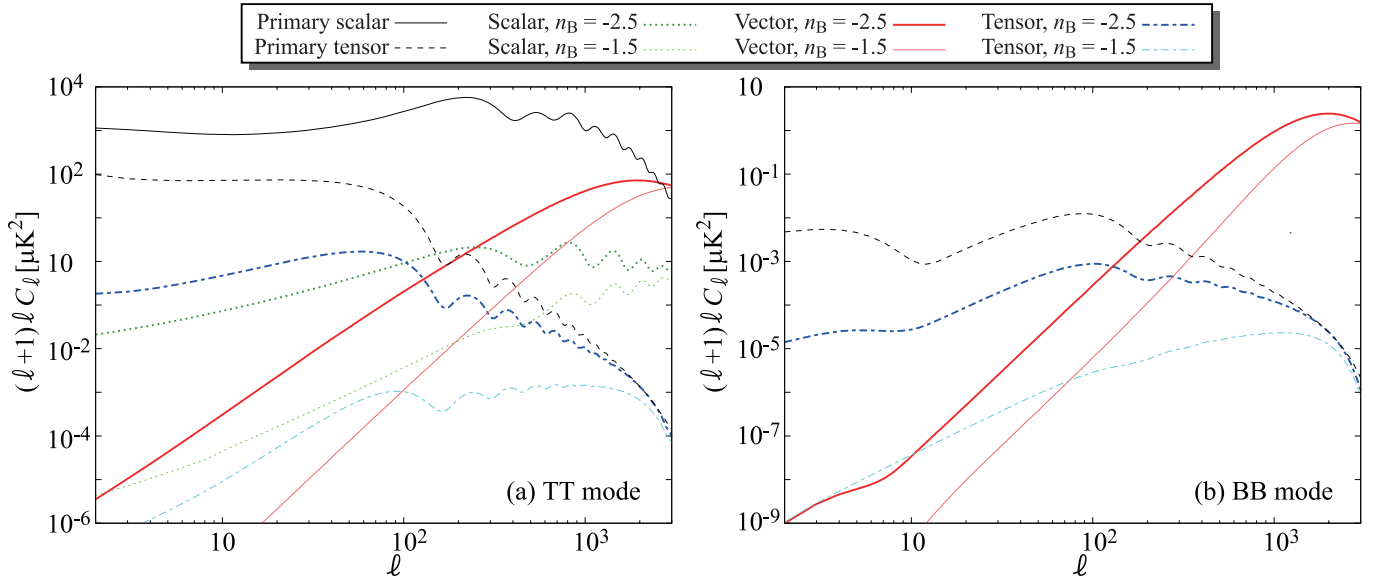


FIG. 4. Polarization anisotropies and temperature fluctuations of CMB the from a PMF. Panels (a) and (b) show TT and BB modes, respectively, for models with $B_\lambda = 3.0$ nG and $n_B = -1.5$ or -2.5 as labeled. We use the scalar to tensor ratio of 0.2 for the primary tensor.

- [48] G. Chen, P. Mukherjee, T. Kahniashvili, B. Ratra, and Y. Wang, *Astrophys. J.* **611**, 655 (2004).
- [49] A. Bernui and W. S. Hipolito-Ricaldi, *Mon. Not. Roy. Astron. Soc.* **389**, 1453 (2008).
- [50] S. K. Sethi, *Mon. Not. Roy. Astron. Soc.* **342**, 962 (2003).
- [51] S. K. Sethi and K. Subramanian, *Mon. Not. Roy. Astron. Soc.* **356**, 778 (2005).
- [52] K. Jedamzik, V. Katalinic, and A. V. Olinto, *Phys. Rev. D* **57**, 3264 (1998).
- [53] K. Subramanian and J. D. Barrow, *Phys. Rev. D* **58**, 083502 (1998).
- [54] R. Banerjee and K. Jedamzik, *Phys. Rev. D* **70**, 123003 (2004).
- [55] M. Bucher, K. Moodley, and N. Turok, *Phys. Rev. D* **62**, 083508 (2000).
- [56] J. R. Shaw and A. Lewis, *Phys. Rev. D* **81**, 043517 (2010).
- [57] K. Yamamoto, N. Sugiyama, and H. Sato, *ApJ*. **501**, 442 (1997).
- [58] T. R. Seshadri and K. Subramanian, *Phys. Rev. Lett.* **87**, 101301 (2001).

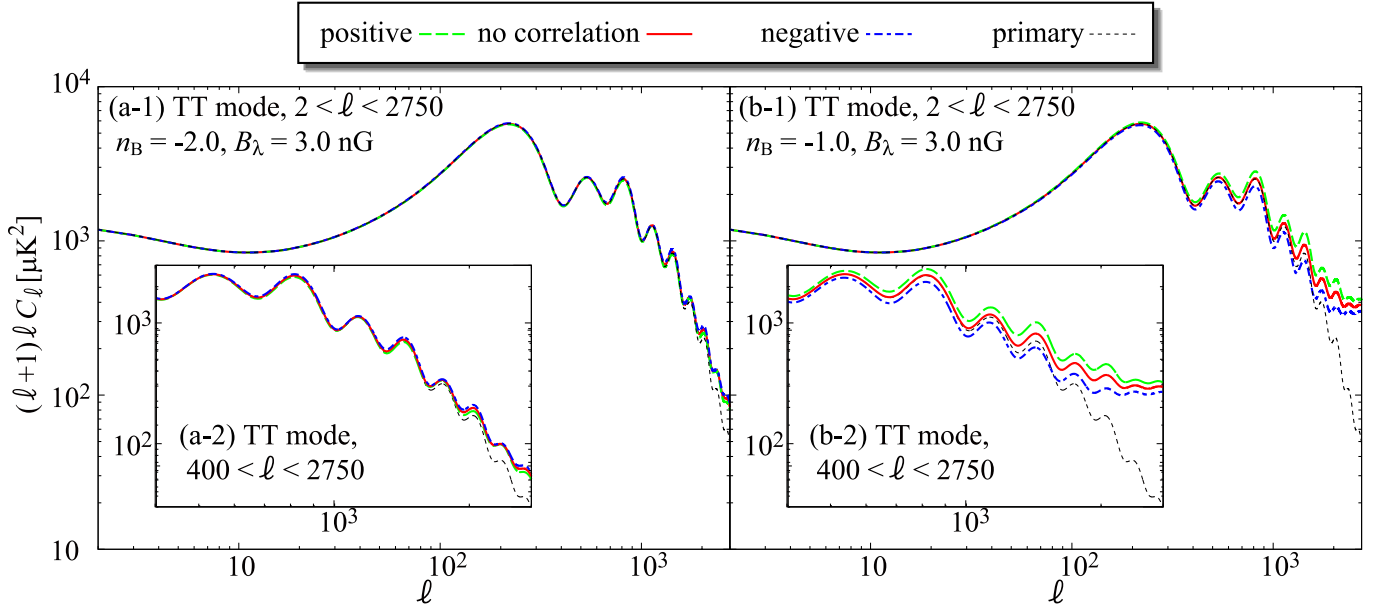


FIG. 5. CMB temperature fluctuations from the PMF. Plots show various ranges for: (a-1) and (b-1) TT($2 < \ell < 2750$), and (a-2) and (b-2) TT($400 < \ell < 2750$) with $B_\lambda = 3.0$ nG and $n_B = -2.0$ (left panel) or -1.0 (right panel). Green dashed, red bold, blue dashed-dotted, and black dotted curves show positive, no and negative correlations, respectively. The black dotted curve shows the primary spectrum without a PMF.

- [59] A. A. Starobinskii, ZhETF Pis ma Redaktsiiu **30**, 719 (1979).
- [60] V. A. Rubakov, M. V. Sazhin, and A. V. Veryaskin, Physics Letters B **115**, 189 (1982).
- [61] A. G. Polnarev, Soviet Astronomy **29**, 607 (1985).
- [62] J. R. Pritchard and M. Kamionkowski, Ann. Phys. **318**, 2 (2005).
- [63] P. J. E. Peebles, *The Large-Scale Structure of the Universe* (Princeton University Press, 1980).
- [64] D. N. Spergel et al. (2006), astro-ph/0603449.
- [65] G. Hinshaw et al. (2006), astro-ph/0603451.
- [66] L. Page et al. (2006), astro-ph/0603450.
- [67] A. Lewis and S. Bridle, Phys. Rev. **D 66**, 103511 (2002).
- [68] S. Cole et al. (The 2dFGRS), Mon. Not. Roy. Astron. Soc. **362**, 505 (2005).
- [69] M. Tegmark et al. (SDSS), Phys. Rev. **D74**, 123507 (2006).
- [70] E. Rozo et al. (2007), astro-ph/0703571.
- [71] A. J. Ross, R. J. Brunner, and A. D. Myers (2008), 0804.3325.
- [72] J. Dunkley et al. (WMAP), Astrophys. J. Suppl. **180**, 306 (2009).
- [73] G. Hinshaw, J. L. Weiland, R. S. Hill, N. Odegard, D. Larson, C. L. Bennett, J. Dunkley, B. Gold, M. R. Greason, N. Jarosik, et al., Astrophys. J **180**, 225 (2009).
- [74] C. L. Kuo, P. A. R. Ade, J. J. Bock, J. R. Bond, C. R. Contaldi, M. D. Daub, J. H. Goldstein, W. L. Holzappel, A. E. Lange, M. Lueker, et al., Astrophys. J. **664**, 687 (2007).
- [75] J. L. Sievers, C. Achermann, J. R. Bond, L. Bronfman, R. Bustos, C. R. Contaldi, C. Dickinson, P. G. Ferreira, M. E. Jones, A. M. Lewis, et al., Astrophys. J. **660**, 976 (2007).
- [76] W. C. Jones et al., Astrophys. J. **647**, 823 (2006).
- [77] C. Caprini and R. Durrer, Phys. Rev. **D 65**, 023517 (2001).
- [78] R. Durrer and C. Caprini, JCAP **0311**, 010 (2003), astro-ph/0305059.
- [79] K. Kojima and K. Ichiki (2009), arXiv:0902.1367.
- [80] R. Durrer, P. G. Ferreira, and T. Kahniashvili, Phys. Rev. **D 61**, 043001 (2000).
- [81] N. Yoshida, N. Sugiyama, and L. Hernquist, Mon. Not. Roy. Astron. Soc. **344**, 481 (2003).

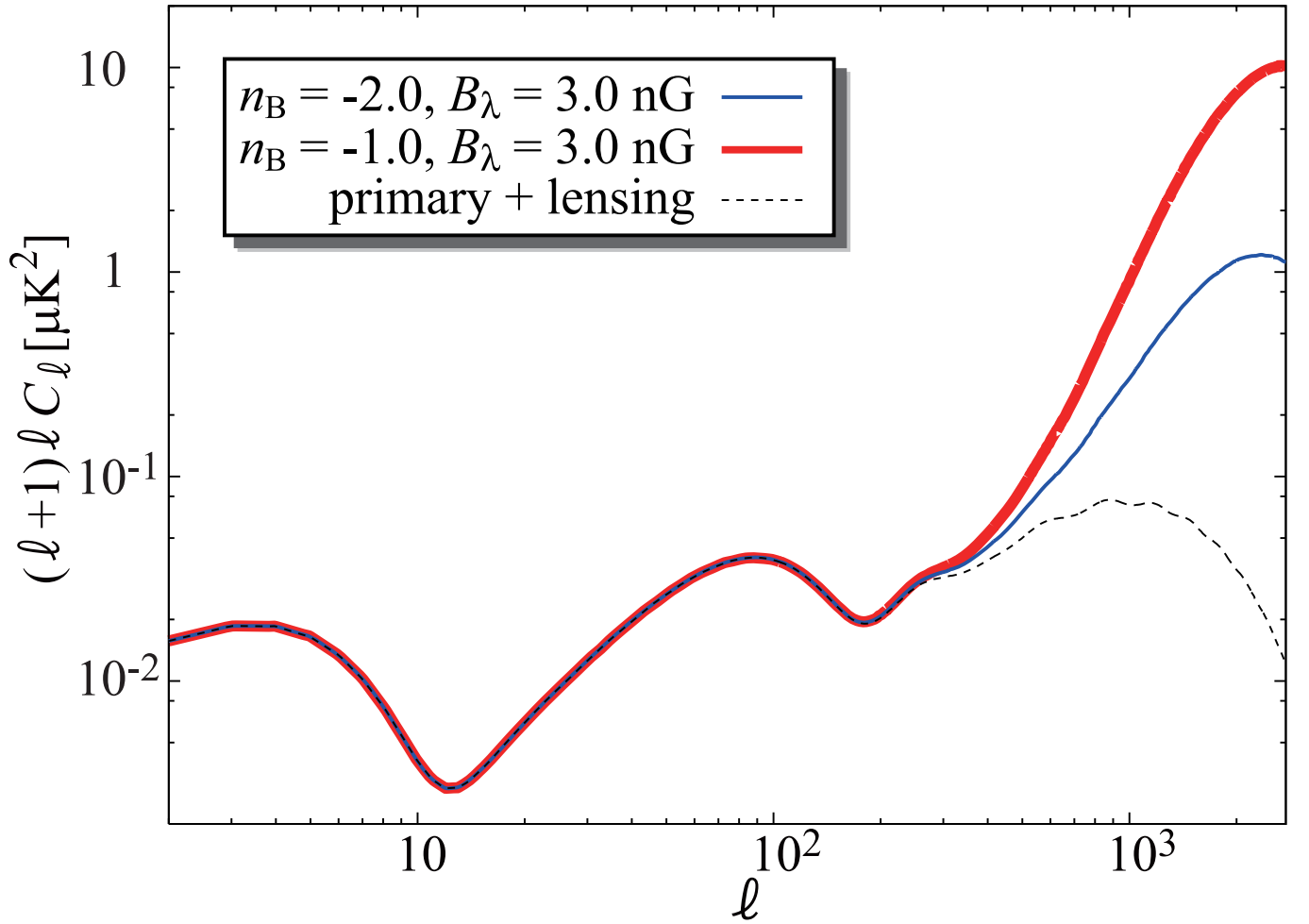


FIG. 6. CMB polarization anisotropies from the PMF. Blue thin and red bold curves show $(B_\lambda, n_B) = (3.0\text{nG}, -2.0)$ and $(B_\lambda, n_B) = (3.0\text{nG}, -1.0)$. The black dotted curve shows a primary spectrum with weak lensing effects (without the PMF).

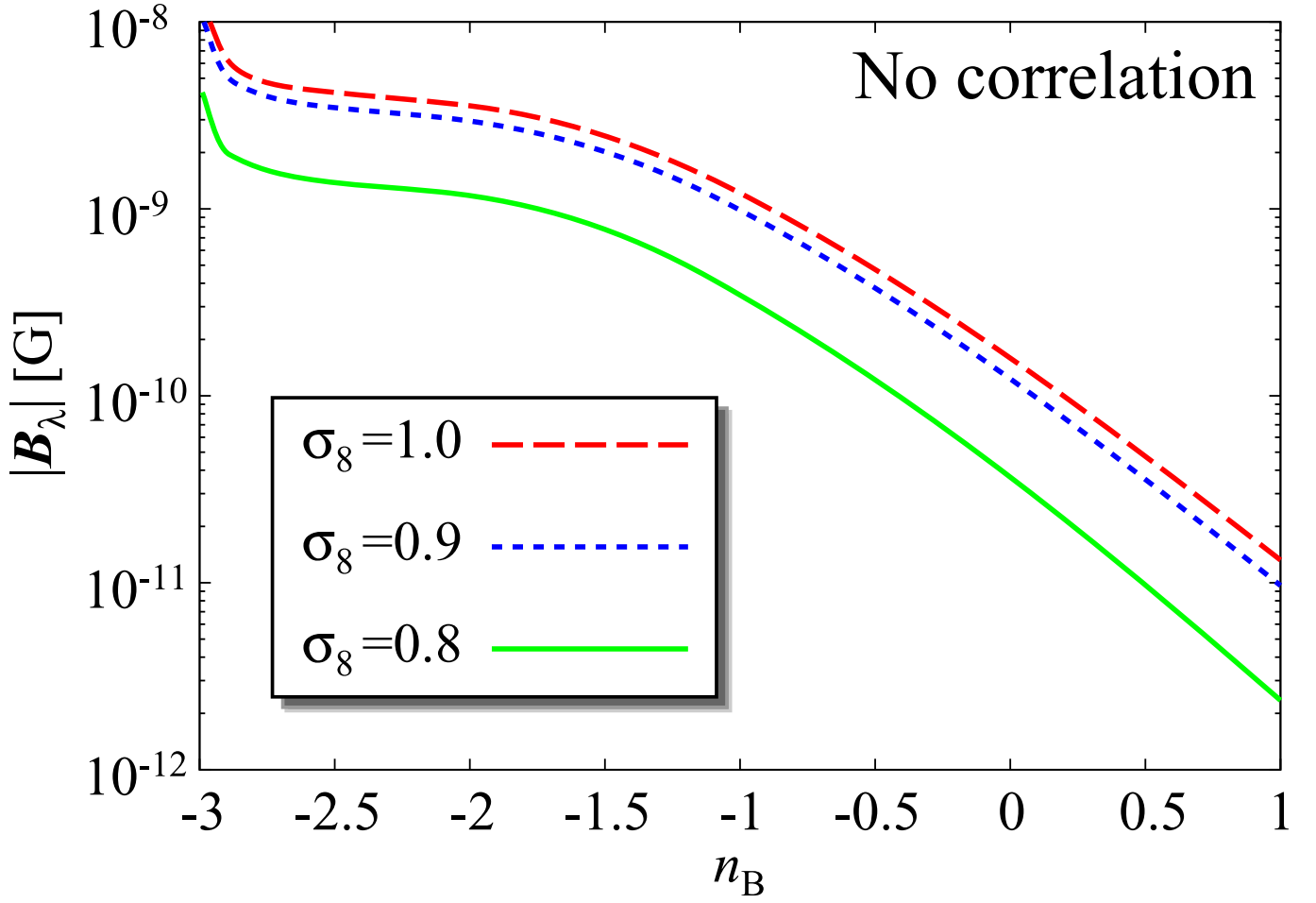


FIG. 7. Curves of constant values for the σ_8 in the parameter plane of PMF amplitude B_λ vs. spectral index n_B for the case of no correlation between the PMF and the matter density fluctuations. Red dashed, blue dotted and green bold curves show constant values of $\sigma_8 = 1.0, 0.9$ and 0.8 , respectively.

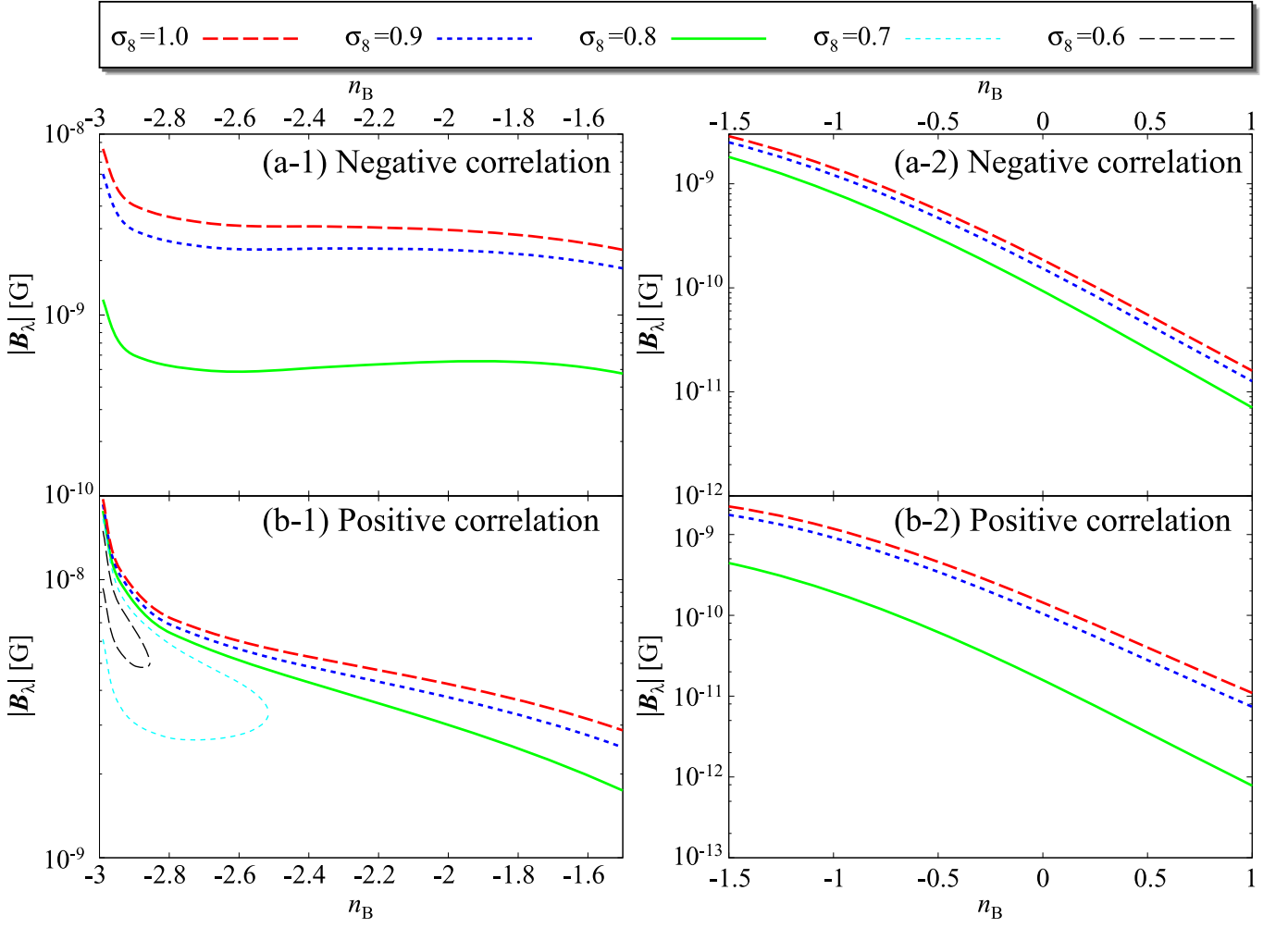


FIG. 8. Curves of constant values for the σ_8 in the parameter plane of PMF amplitude B_λ vs. spectral index n_B for the negative ($s_{\text{DF}} = -1$) and positive ($s_{\text{DF}} = 1$) correlations between the PMF and the matter density fluctuations. Panels (a-1) and (b-1) show $n_B < -1.5$ as the PMF pressure dominated region. On the other hand, panels (a-2) and (b-2) show $n_B > -1.5$ as the PMF tension dominated region. Red dashed, blue dotted, green bold, azure dotted thin, and black dashed thin curves show constant values of $\sigma_8 = 1.0, 0.9, 0.8, 0.7$ and 0.6 , respectively.

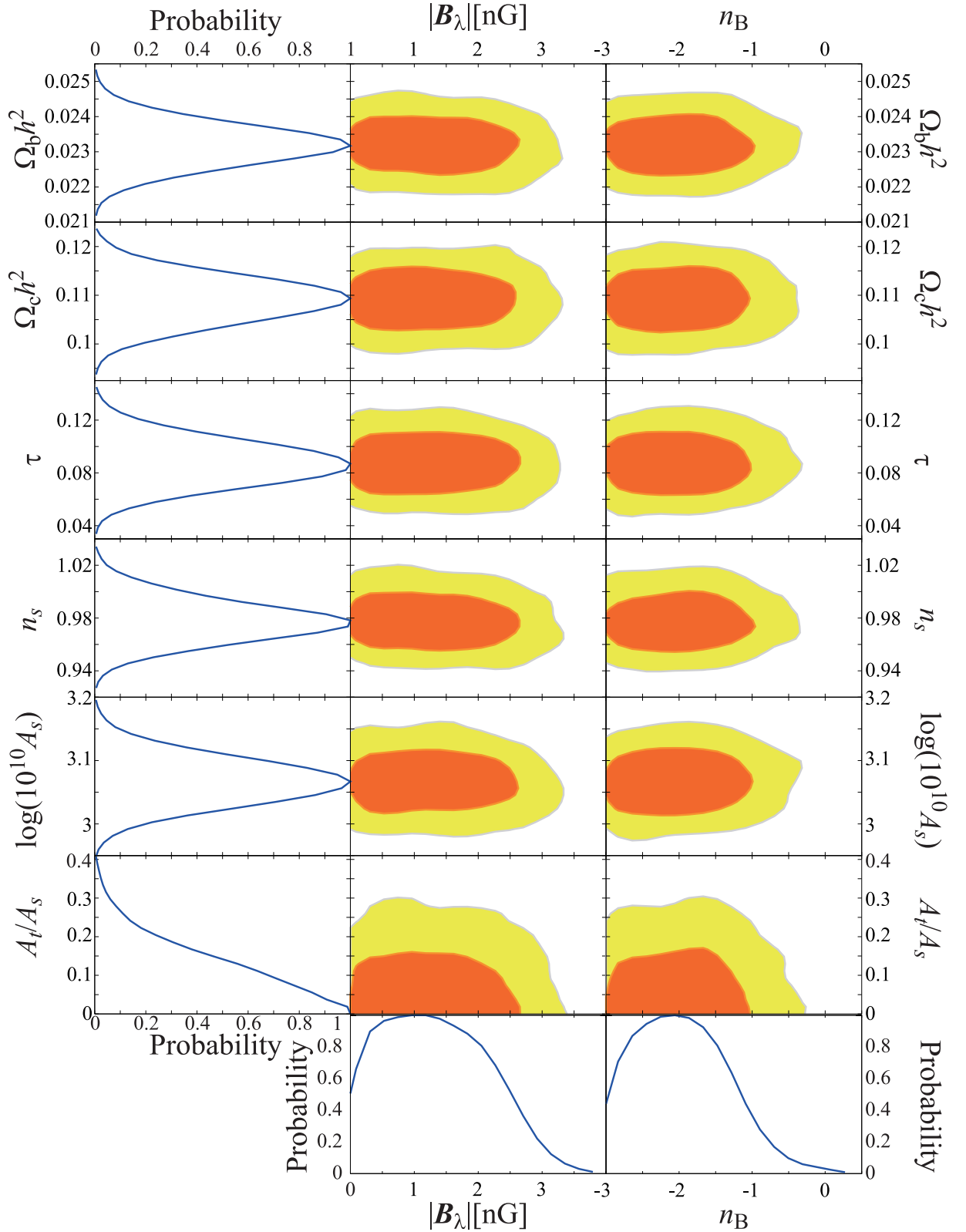


FIG. 9. Probability distributions and contours of 1σ and 2σ confidence limits for the standard cosmological parameters as a function of the PMF field strength $|B_\lambda|$ and power law index n_B . Orange contours show 1σ (68%) confidence limits and yellow contours show 2σ (95%) confidence limits. Blue curves in the left and bottom of the figure show the probability distributions of each parameter. Note the existence of a maximum in the probability distributions for $|B_\lambda|$ and n_B . The standard cosmological parameters do not have a degeneracy with the PMF parameters because they are mainly constrained by the observed CMB data for $\ell < 1000$ (up to the 2nd peak), while the PMF is mainly influenced by the power on smaller angular scales and higher multipoles, $\ell > 1000$.

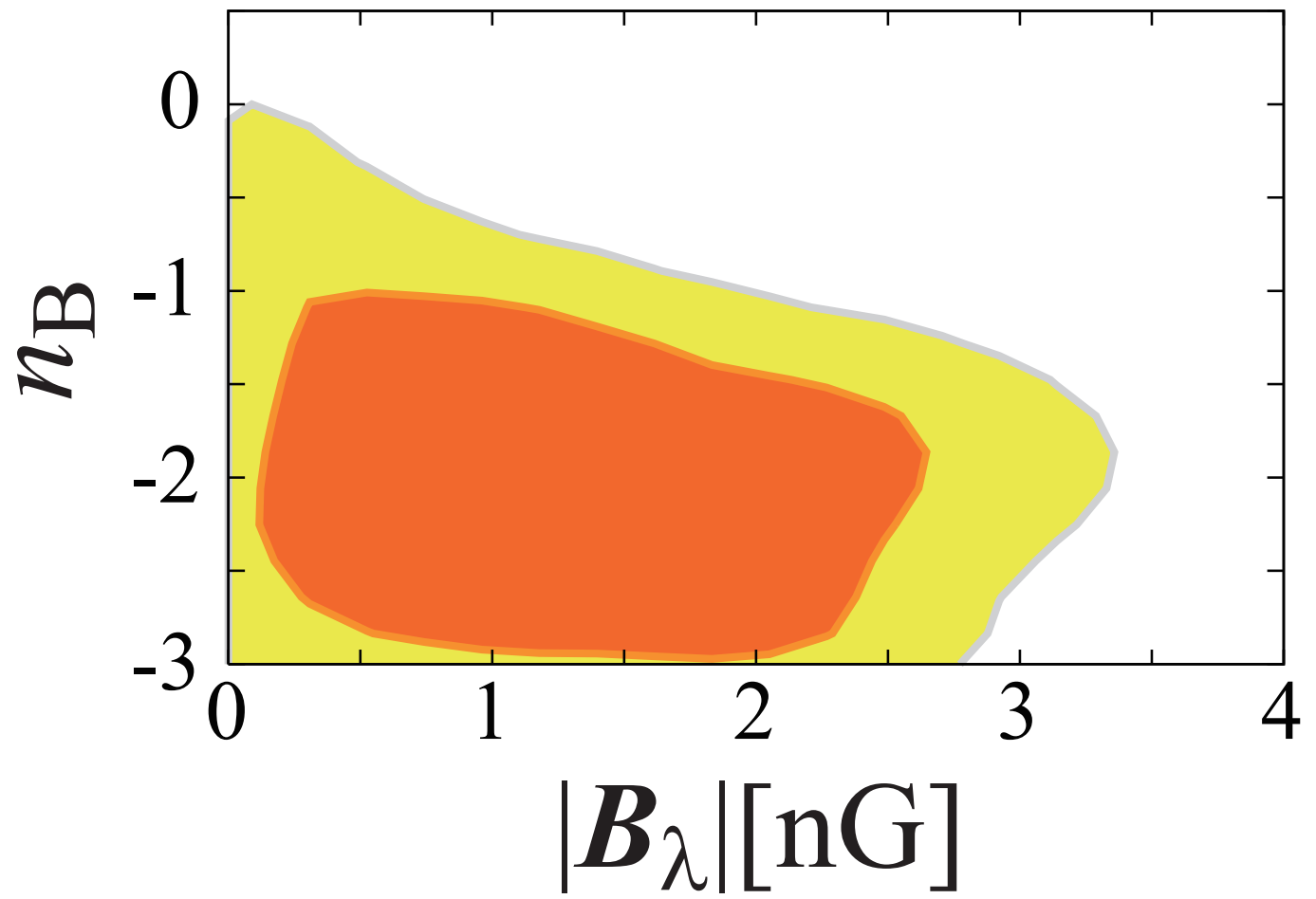


FIG. 10. Probability contours in the plane of B_λ vs. n_B . Orange contours show 1 σ (68%) confidence limits and yellow contours show 2 σ (95%) confidence limits.

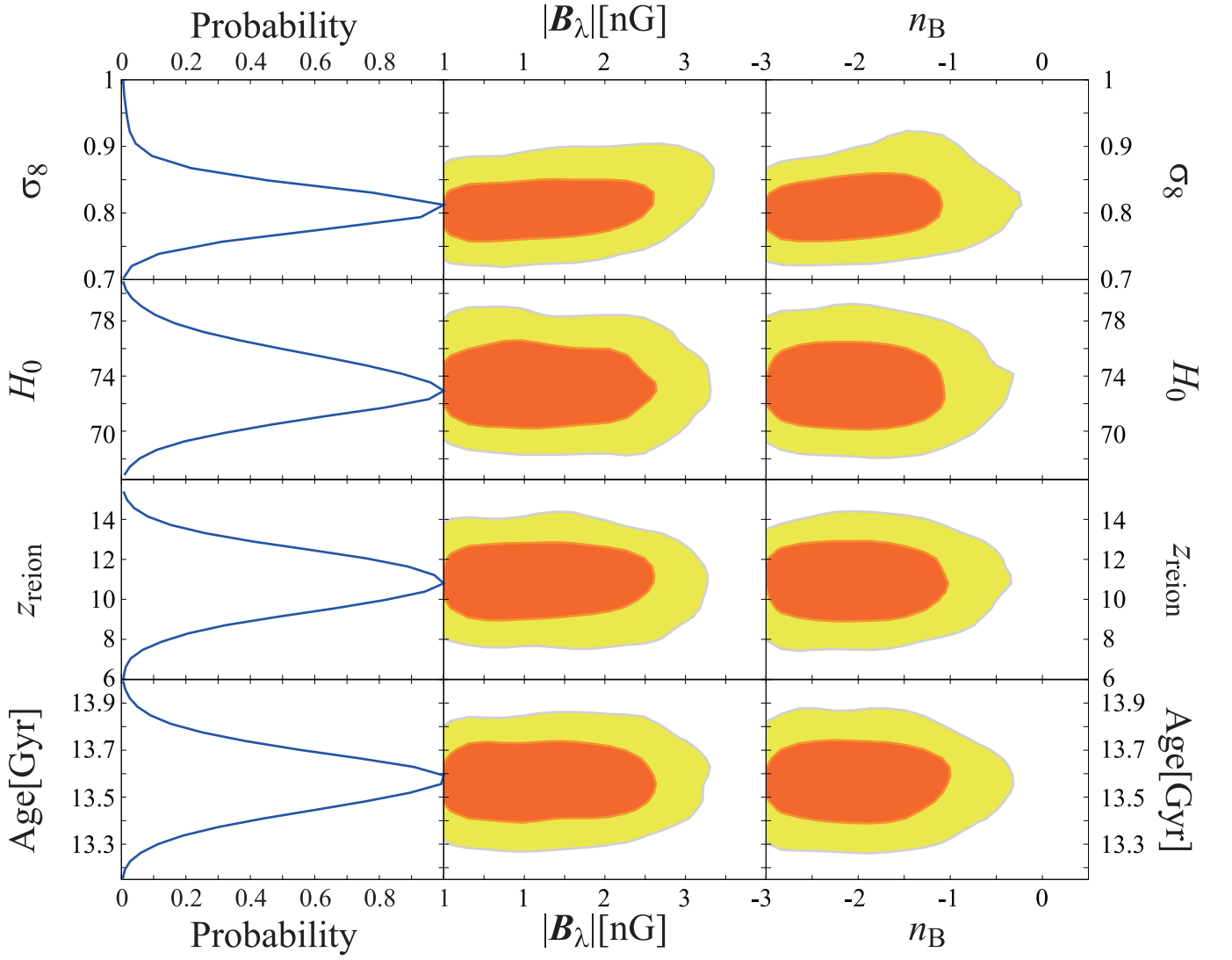


FIG. 11. Probability distributions and contours of 1σ and 2σ confidence limits for the parameters σ_8 , H_0 , z_{reion} and Age. Orange contours show 1σ (68%) confidence limits and yellow contours show 2σ (95%) confidence limits. Blue curves show probability distributions for each parameter. Note that these are not input priors, but output results.

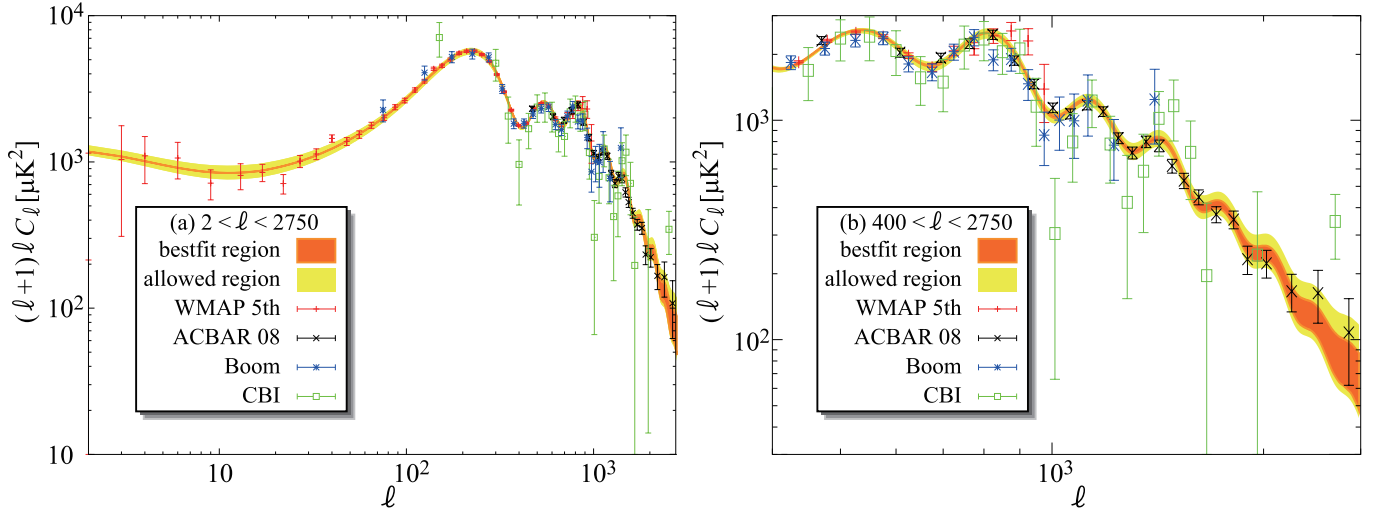


FIG. 12. Comparison of the best-fit computed total power spectrum with the observed CMB spectra. Plots show various ranges for: (a) TT($2 < \ell < 2750$) and (b) TT($400 < \ell < 2750$) modes. Orange regions are from the best-fit parameter set and allowed regions are from constrained parameter set as Table.1. Red, black, blue, green, orange, and purple dots with error bars show WMAP 5yr, ACBAR 08, Boomerang and CBI data, respectively. Since the SZ effect depends upon frequencies of the CMB for the TT mode, we plot the best fit and allowed regions in panels (a) and (b) surrounded by the curves with the SZ effect at the K(22.8GHz) band (upper curves) and without the SZ effect(lower curves).

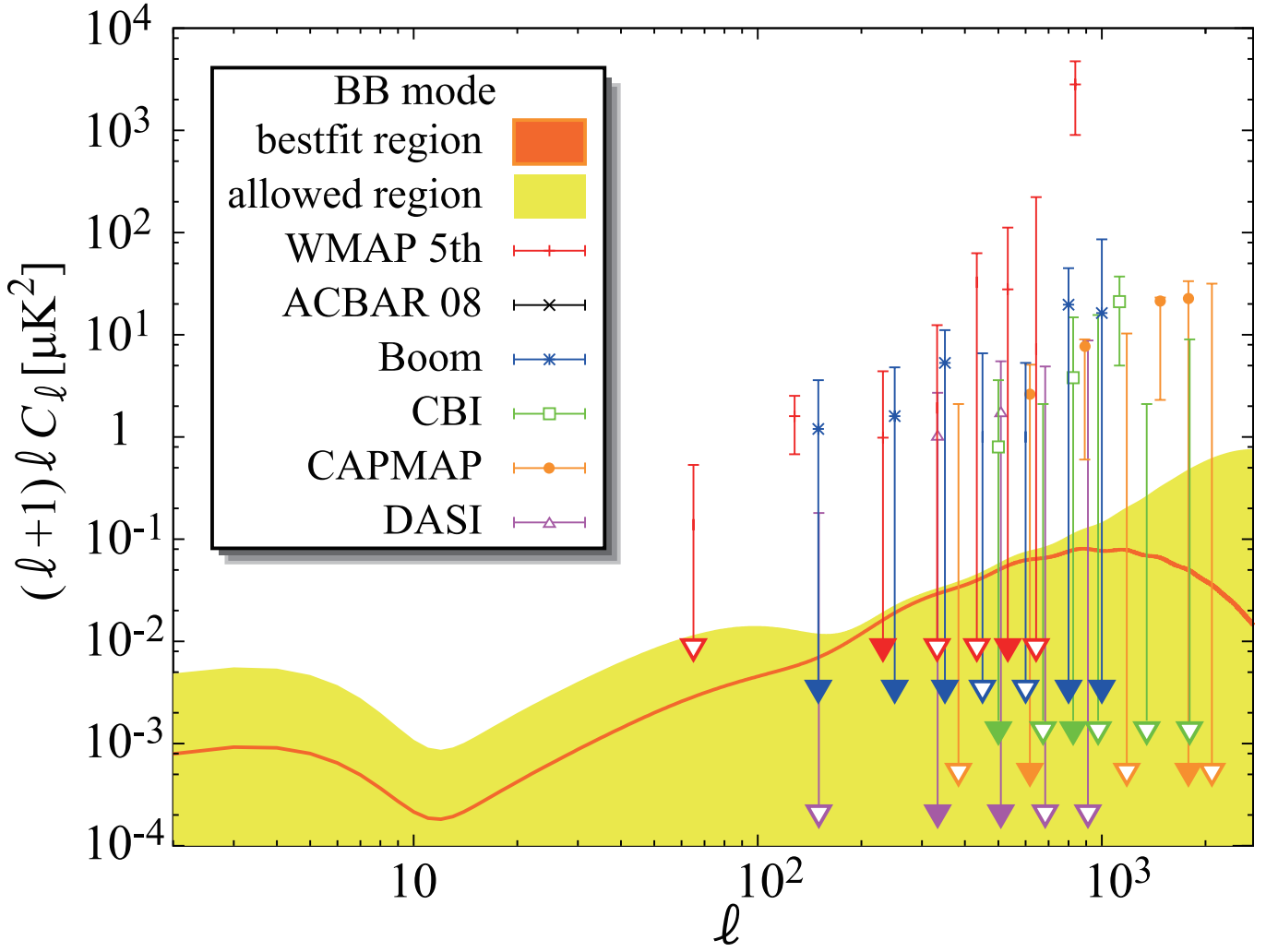


FIG. 13. Comparison of the best-fit computed total power spectrum with the observed CMB spectra. The orange region is from the best-fit parameter set and the allowed region is from the constrained parameter set as given in Table.1. Red, black, blue, green, orange, and purple dots with error bars show WMAP 5yr, ACBAR 08, Boomerang, CBI, CAPMAP, and DASI data, respectively. Downward arrows for the error bars on this figure indicate that the data points are upper limits. Since the BB mode is not affected by the SZ effect, the upper curves and lower curves in this figure are defined by the constrained cosmological parameters of Table.1.